UNIVERSIDADE FEDERAL DO RIO GRANDE DO SUL
INSTITUTO DE PESQUISAS HIDRÁULICAS
PROGRAMA DE PÓS-GRADUAÇÃO EM RECURSOS HÍDRICOS E SANEAMENTO AMBIENTAL

Cayo Lopes Bezerra Chalegre

Pareamento de Processos Bacia-Lagoa: Desenvolvimento de modelo hidrodinâmico de fluxos subsuperficiais e superficiais acoplados

Porto Alegre
2021

Cayo Lopes Bezerra Chalegre

Pareamento de Processos Bacia-Lagoa: Desenvolvimento de modelo hidrodinâmico de fluxos subsuperficiais e superficiais acoplados

Dissertação apresentada ao Programa de Pós-Graduação em Recursos Hídricos e Saneamento Ambiental da Universidade Federal do Rio Grande do Sul, como requesito parcial à obtenção do grau de Mestre.

Orientador: David da Motta Marques

Porto Alegre

2021

CIP - Catalogação na Publicação

Chalegre, Cayo Lopes Bezerra
Pareamento de Processos Bacia-Lagoa: Desenvolvimento de modelo hidrodinâmico de fluxos subsuperficiais e superficiais acoplados / Cayo Lopes Bezerra Chalegre. -- 2021.
49 f.
Orientador: David da Motta Marques.

Dissertação (Mestrado) -- Universidade Federal do Rio Grande do Sul, Instituto de Pesquisas Hidráulicas, Programa de Pós-Graduação em Recursos Hídricos e Saneamento Ambiental, Porto Alegre, BR-RS, 2021.

1. Modelagem de escoamento subsuperficial. 2. Modelagem de escoamentos acoplados. 3. Modelo IPH-ECO. I. Marques, David da Motta, orient. II. Título.

Elaborada pelo Sistema de Geração Automática de Ficha Catalográfica da UFRGS com os dados fornecidos pelo(a) autor(a).

Cayo Lopes Bezerra Chalegre

Pareamento de Processos Bacia-Lagoa: Desenvolvimento de modelo hidrodinâmico de fluxos subsuperficiais e superficiais acoplados

Dissertação apresentada ao Programa de Pós-Graduação em Recursos Hídricos e Saneamento Ambiental da Universidade Federal do Rio Grande do Sul, como requesito parcial à obtenção do grau de Mestre.

Trabalho aprovado. Porto Alegre, 24 de Maio de 2021.

Prof. Dr. David da Motta Marques– UFRGS
Orientador

Prof. Dr. Fernando Mainardi Fan – UFRGS
Examinador

Prof. Dr. Juan Martín Bravo – UFRGS
Examinador

Prof. Dr. Cristovão Vicente Scapulatempo Fernandes – UFPR
Examinador

Agradecimentos

Esse período (2020-2021) foi atípico para o mundo todo e acredito que não deveria iniciar meus agradecimentos se não agradecendo as ações Dele. Agradeço a Ele pelos caminhos iluminados para alcançar as minhas realizações pessoais. Mas, o mais importante, agradeço pelos momentos reconfortantes que Ele nos enviou em meio a perdas, desesperança e angústia passadas por nós e pelas famílias das 3.2 milhões de filhos, irmãos e pais que foram levados a Seu encontro.

Aos professores David da Motta-Marques e Carlos Ruberto Fragoso Jr. pelo entusiasmo e toda troca de conhecimento ao longo desse período de trabalho. Além disso, agradeço a amizade construída ao longo desse processo.

Aos membros da banca examinadora Prof. Fernando Mainardi Fan, Prof. Juan Martín Bravo e Prof. Cristovão Vicente Scapulatempo Fernandes pelas contribuições ao trabalho.

Ao Instituto de Pesquisas Hidráulicas-IPH por propiciar estrutura e ambiente adequada para a capacitação e troca de conhecimento entre seus membros.

Ao CNPq pelo suporte financeiro e bolsa de pesquisador concedida (número da bolsa: 132643/2019-7).

Ao apoio e carinho dos meus familiares. Aos meus pais Rita e Agildo. À minha irmã Camyle. À minha avó Edelvita e minha Tia Ana.

Aos meus amigos: Léo, Bruno, Larissa, Thainá, Jéssica e Júlio. E, meus amigos e companheiros de laboratório: Matheus, Itzaiana e Hugo. Todos foram responsáveis por tornarem Porto Alegre um novo lar e facilitar a construção desse trabalho.

À Mari pela mais pura amizade, companheirismo e apoio em todos os momentos.

Resumo

Ambientes lacustres são bastante suscetíveis aos processos que ocorrem em sua bacia hidrográfica tornando a análise acoplada bacia-lagoa essencial no entendimento de sua estrutura e funcionamento. Dentre esses processos, a interação entre o escoamento superficial e subsuperficial pode exercer forte influência no balanço hídrico e de nutrientes desses ecossistemas. Contudo, a heterogeneidade espacial e temporal da distribuição desses fluxos pode tornar o processo de quantificação dificultoso e a aplicação de técnicas convencionais pode não ser compensatória. Muitas dessas técnicas tem uma abrangência espacial e temporal limitadas. Contudo, a combinação entre métodos convencionais com a modelagem dos fluxos acoplados pode ser uma abordagem adequada para lidar com essa heterogeneidade, possibilitando avaliar a interação entre ambos os escoamentos. Nesse estudo, iniciamos a expansão do modulo hidrodinâmico do modelo hidrodinâmico e ecológico IPH-ECO, visando consolidá-lo como ferramenta cientifica com objetivo de permitir a avaliação dessa dinâmica para ambientes lacustres subtropicais. Implementamos um esquema numérico híbrido de volumes finitos e diferenças finitas de forma a permitir a modelagem acoplada de ambos os fluxos. Os fluxos foram acoplados considerando as hipóteses de Dupuit válidas, integrando-os através de uma condição de contorno cinemática na interface entre ambos. O algoritmo proposto foi testado através de três *benchmarks* comumente usados para validação desse tipo de metodologia. Bons resultados foram encontrados para dois *benchmarks*, demonstrando a capacidade do modelo em simular fluxos bem-desenvolvidos acoplados através de uma barragem porosa e a influência da maré em um ambiente lagunar costeiro separado do mar por uma faixa litorânea sedimentar. No terceiro *benchmarks* uma bacia com um curso d'água de drenagem foi simulado considerando dois cenários, o primeiro considerando apenas fluxo superficial e o segundo fluxos acoplados. A simulação do cenário onde somente escoamento superficial foi simulado demonstrou bons resultados quando comparados a modelos anteriores. A simulação do segundo cenário permitiu a identificação de algumas limitações da nova abordagem durante o processo de saturação e transição entre os escoamentos subsuperficiais e superficiais. A análise mais aprofundada de estudos anteriores demonstra a necessidade de adoção de metodologias complementares para assegurar uma rigorosa conservação da massa nessa etap. Entre essas metodologias o uso de um algoritmo de passo de tempo adaptativo para o modulo hidrodinâmico e a adoção da resolução de sub-grid se mostram como soluções adequadas para lidar com essas limitações. Com isso, pretendemos abordar estas limitações em estudos complementares de forma a alcançar a consolidação do novo módulo hidrodinâmico do modelo IPH-ECO.

Palavras-Chave: escoamentos acoplados, escoamento subsuperficial, modelo IPH-ECO.

Abstract

Lake ecosystems are highly susceptible to the processes that occur in their catchment area, and coupling watershed-lake modeling is critical to understand better lakes' structure and functioning. The interaction between surface and subsurface flows can significantly influence the water and nutrient balance of these ecosystems. However, the spatial and temporal heterogeneity of the flow distribution makes the quantification process difficult, and the application of the conventional techniques might not be adequate. Many of these methods have limited spatial and temporal coverage. Thus, conventional methods combined with coupled modeling of these flows may be a suitable approach to deal with this heterogeneity, allowing assess the interaction between both flows. In this study, we expanded the IPH-ECO's model hydrodynamic module to consolidate it as a scientific tool to simulate subsurface-surface flow dynamics for subtropical lake environments. We implemented a hybrid finite volume and finite difference numerical scheme to allow coupled modeling of both flows. The flows were coupled considering the valid Dupuit hypothesis, integrating the flows through a kinematic boundary condition at the interface between them. The proposed algorithm was validated using three benchmarks commonly used for validation of this type of approach. Successful results were found for two benchmarks, demonstrating the model's ability to simulate well-developed coupled flows through a porous dam and tidal influence in a coastal lagoon environment separated from the sea by a sediment bank. In the third benchmark, we simulated a catchment with a river channel considering two scenarios, the first one considering only surface flow and the second one coupled flows. The first simulated scenario showed good results when compared to the previous model results. The simulation of the second scenario allowed the identification of some limitations of the new approach during the saturation process and transition between subsurface and surface runoff. Further analysis of previous studies demonstrates a need for complementary methodologies adoption to ensure rigorous mass conservation at this point. Of those methodologies, an adaptive time-step algorithm and the adoption of sub-grid resolution seem to be adequate solutions to deal with these limitations. Thus, we will address these limitations in further studies to consolidate the new hydrodynamic module of the IPH-ECO model.

Key-words: coupled flows, subsurface flow, IPH-ECO model.

List of Figures

List of symbols

Ω	Numerical Domain
s	Soil level
h	Impervious Bottom Level
x, y, z	Cartesian coordinates
u	Velocity in x-axis direction
v	Velocity in y-axis direction
w	Velocity in z-axis direction
f	Coriolis parameter
Pa	Atmospheric Pressure
η	Free-Surface Elevation/Phreatic level
g	Gravitational acceleration
q	Non-hydrostatic pressure component
ν^h	Eddy horizontal viscosity coefficient
ν^v	Eddy vertical viscosity coefficient
$\triangle$	Laplacian operator
γ_T	Wind stress coefficient
u_a	Wind velocity in x-axis direction
v_a	Wind velocity in y-axis direction

γ_B	Bottom friction coefficient
u^*	Velocity component tangential at the sediment-water interface in x-axis direction
v^*	Velocity component tangential at the sediment-water interface in y-axis direction
V^g	Subsuperficial velocity vector
$\mathcal{K}$	Soil hydraulic conductivity
$\triangle_h$	Horizontal laplacian operator
u^g	Subsuperficial velocity in x-axis direction
v^g	Subsuperficial velocity in x-axis direction
Θ	Soil moisture content
ϵ	Soil porosity
S	Water saturation
$\mathcal{H}$	Heaviside step-function
Ω_i	i-th polygon in numerical Domain
P_i	i-th Polygon area
N_p	Number of polygons
N_s	Number of polygon sides
Γ_j	j-th Polygon side
$\lambda_{j,k+\frac{1}{2}}$	j-th Discrete Polygon side length at k+1/2 layer
$\wp_{(i,j)}$	Neighbor of polygon $i-th$ that share side j-th
δ_j	Distance between centers of two adjacent polygons with share j-th side
z_k	Discrete layer level at k-th layer
Δz_k	Discrete layer thickness at k-th layer
$\Delta \bar{z}^n_{j,k}$	Discrete superficial layer thickness at j-th side and k-th layer
$\Delta \tilde{z}^n_{j,k}$	Discrete subsuperficial layer thickness at j-th side and k-th layer
t_n	Simulation time at n-th time-step

$a_{j,k}^{n}$	Discrete total wet area thickness at j-th side and k-th layer
$\bar{a}_{j,k}^{n}$	Discrete superficial wet area thickness at j-th side and k-th layer
$\tilde{a}_{j,k}^{n}$	Discrete subsuperficial wet area thickness at j-th side and k-th layer
$\bar{u}_{j}^{n+1}$	Discrete normal superficial velocity component at j-th edge and k+1/2 layer
$\tilde{u}_{j}^{n+1}$	Discrete normal subsuperficial velocity component at j-th edge and k+1/2 layer
$u_{j,k}$	Discrete normal velocity component at j-th edge and k-th layer
$w_{i,k+1/2}$	Discrete vertical velocity component at i-th element and k+1/2 layer
F	Explicit finite difference operator
η_i	Discrete free-surface elevation/phreatic level at i-th element
θ	Implicitness parameter from θ-method
Δt	Time-step
$\nu_{j,k+1/2}$	Discrete eddy horizontal viscosity coefficient at j-th edge and k-th layer
$u_{j,k}^{*}$	Discrete superficial velocity in x-axis direction interpolated at end of Lagragian path
$v_{j,k}^{*}$	Discrete superficial velocity in y-axis direction interpolated at end of Lagragian path
$\mathcal{K}_{j,k}$	Discrete soil hydraulic conductivity at j-th edge and k+1/2 layer
$V\left(\eta_i^{n+1}\right)$	Discrete water volume at i-th element
$\sigma_{i,j}$	Sign function associated with the orientation of the normal velocities
Δx	Numerical discretization in x-axis direction
Δy	Numerical discretization in y-axis direction
a	Tidal amplitude
T	Tidal period

Contents

Chapter 1

Introduction

Lake ecosystems play an important role as providers of ecosystem services to society. These environments have a strong dependence on hydrological and anthropogenic processes in their watershed, making the integrated analysis of lake ecosystems more effective in understanding their dynamics. Subsurface waters are a significant component of these integrated dynamics that are often considered negligible. However, the relevance of the impact of this component on the water quality and quantity of these ecosystems has been observed in several studies (Hagerthey e Kerfoot, 1998; Zhu e Schwartz, 2011; Oliveira Ommen et al., 2012; Shaw et al., 2013).

The challenge in quantifying the magnitude of these subsurface changes is one of the major reasons that this process has been neglected. The distributions of exchange between subsurface and a lake are heterogeneous both spatially and temporally. Moreover, this heterogeneity exists at different scales. The spatial heterogeneity at basin scale will depend on geological formations, aquifer characteristics, and its recharge (Winter, 1978; Schneider et al., 2005). While on a local scale (in lakes) this interaction will mainly depend on the heterogeneity of soil characteristics (at the lake bottom and shore) (Pfannkuch e Winter, 1984; Cherkauer e Nader, 1989; Genereux e Bandopadhyay, 2001; Kishel e Gerla, 2002; Kidmose et al., 2011, 2013). Moreover, the temporal seasonality of this discharge can be varied across different periods of the year. All these factors make accurate discharge quantification difficult, and this process can depend on the application of multiple measurement methods.

In this context, within the possible methodologies applied to the quantification of these exchanges, the use of integrated subsurface-surface flow models is an alternative methodology to overcome these difficulties. In this context, the present study takes the

first step towards expanding the hydrodynamic and ecological model IPH-ECO to enable the coupled simulation of these flows in subtropical continental water environments. In the subsequent items of this chapter, the following topics will be covered: a brief approach on the interaction and quantification methods of these fluxes; coupled simulation methodologies; presentation of the IPH-ECO model; and the objectives and organization of this study.

1.1 Subsurface-Surface flows interaction

The subsurface flows can play a relevant role in the water budget of lake ecosystems. In some lakes, its contribution rates can be as high as 94% of the entire balance (Rosenberry et al., 2015). This occurs in sites that have high rates of gain by exfiltration (i.e., subsurface flow to the lake) (Rosenberry, 2000; Gurrieri e Furniss, 2004; Nakayama e Watanabe, 2008; Stets et al., 2010; Kidmose et al., 2013) or infiltration (i.e., flow from the lake to the subsurface reservoir) (Winter e Likens, 2009; Zhou et al., 2013). The quantification of these fluxes is neglected in several cases because they are considered irrelevant compared to other water budget terms. However, studies indicate that this interaction is relevant in environments without surface outflow or when the evaporation rate exceeds precipitation (Nakayama e Watanabe, 2008; Lewandowski et al., 2015). Also, for instance, in the case of large lakes, the flow area can be extensive, implying that the volume changed can be high even at low rates (Rosenberry et al., 2015).

The nutrient budget is also another relevant aspect in this interaction since there are a greater variety and higher concentrations of nutrients in subsurface waters than in surface ones (Hem, 1985; Drever et al., 1988; Appelo e Postma, 2004; Lewandowski et al., 2015). Besides the nutrients naturally present in the soil, subsurface flows are also responsible for the transport of nutrients from diffuse and point soil pollution sources, which is mainly due to anthropogenic activities (e. g. such as contamination of water pumping wells, leakage of contaminants, or use of fertilizers in agriculture). Within this context, the interaction between surface and subsurface waters is more complex, as its relevance depends on the spatial-temporal distribution patterns of water and the concentrations of nutrients exchanged (Kenoyer e Anderson, 1989; LaBaugh et al., 1997; Sutula et al., 2001). This implies that the nutrient exchange can play a very significant role in the ecological dynamics of these ecosystems in cases in which the volume of exchanged water is low, or when the exfiltration/infiltration net is zero.

It is observed that the subsurface-surface flows interaction can produce effects that can be severely damaging to these ecosystems, such as an increase in their toxicity due to the eutrophication process (Brauns et al., 2016). Nevertheless, there are also cases where excess exchanged nutrients can induce beneficial responses, such as high anammox rates (i.e., ammonium oxidation by autotrophic bacteria in anoxic condition) (Zhu et al., 2013),

which may have a positive effect on inducing high nitrogen loss (Xu et al., 2009; Zhu et al., 2013; McCarthy et al., 2016; Brauns et al., 2016). Thus, it is clear that quantifying spatially and temporally these fluxes (both volumetric and nutrient) and understanding the processes involved is essential in developing an effective management process of these ecosystems, allowing the prediction of potential risks to the ecosystem services provided, as well as potential gains.

1.2 Subsurface flow quantification

Different methods can be applied to quantifying the coupled fluxes between subsurface and surface flows. These methods can be based on water or nutrient balances; on the use of chemical and biological tracers (Malard et al., 1996; Wetzel, 1999; Sebestyen e Schneider, 2001; Santos et al., 2008; Shaw et al., 2013; Rautio e Korkka-Niemi, 2015); temperature and thermal gradient analysis (Baskin, 1998; Kang et al., 2005; Anderson, 2005; Anibas et al., 2009; Briggs et al., 2012; Sebok et al., 2013); direct measurement methods (e. g. seepage meters); as well as based on mathematical modeling (Winter et al., 2003; Lake, 2013; Yihdego e Becht, 2013). Some of these methods are employed only to identify the potential interaction zones between these flows, while others estimate the exchanged volumes.

The quantification accuracy depends directly on the method chosen since each has an uncertainty associated with each one. These uncertainties increase due to the spatial and temporal extent of the collected data. Some methods only take punctual measurements. Thus, there is a need to extrapolate measurements temporally and spatially to the entire lake. Studies have shown that differences in estimates from different ones for same location can reach more than 100% (see LaBaugh et al. 1997; Lee e Swancar 1997; Meinikmann et al. 2013). Adopting several methods in the same study is an appropriate manner to minimize the uncertainty associated with the methodologies. For instance, in Ala-Aho et al. (2013) the character of the subsurface-lake interactions are estimated using chemical tracers, hydraulic head, and seepage meter measurements. Wilson e Rocha (2016) combined Landsat Thematic Mapper/Enhanced Thematic Mapper Plus (TM/ETM+) thermal imaging and geochemical plotters (radium and water conductivity), obtaining satisfactory results in defining these zones in Lake Lough Mask, Ireland. On a regional scale, Ala-Aho et al. (2015) used a fully integrated surface-subsurface model to evaluate the groundwater interaction in Esqker Aquifer, validating using thermal images and stable isotopes data collected in situ.

Numerical modeling can be a complementary method to deal with spatial and temporal range limitations from other methods. However, its application may also be constrained due to limitations in acquiring representative field data from study site or by

to computational cost (Beven, 2002). The field data play a relevant role provide input and validation information to the model. And, usage of complementary methodologies, such as those cited above, can handle it. Whereas, the computational cost reduction can be associate with simplification assumptions about the processes involved in the simulation (e.g., assuming predominantly two-dimensional flow, hydrostatic pressure, homogeneous soil parameters), providing results that are similarly accurate to those of a more "complex" approach and allowing for more practical applications (e.g., Gunduz e Aral (2005); Liang et al. (2007); Kong et al. (2010); Casulli (2015); Chen et al. (2020)).

1.3 Coupled subsurface-surface modeling approaches

The subsurface-surface modeling has been done using a decoupled non-iterative and iterative models and coupled models (Huang e Yeh, 2009; Chen et al., 2020; Wu et al., 2021). The non-iterative models (simplest way) use the results of two models (one model to simulate each flow), adopting the output of the subsurface flow model as the boundary condition of the surface flow model. Whereas, in the decoupled iterative methodology, the different models integrate at the time step level. This methodology can improve accuracy, but there is still no guarantee that the results will be as accurate as coupled methodologies. Coupled methodologies solve the equations for subsurface and surface regimes simultaneously, integrating both flows from a kinematic boundary condition at the interface between the domains of each. This approach minimize convergence and mass conservation problems that often occur mainly in the presence of wetting/drying dynamics, in non-homogeneous porous media, and during the free-surface transition at the interface of both flows (Weill et al., 2009; Casulli e Zanolli, 2010; Casulli, 2015; Chen et al., 2020).

The set of equations adopted by the models is a significant point to must be observed in the modeling process. There are models with higher sophistication that use 3D approximations for both flows, applying the Navier-Stokes equations for surface flow and the Richards equation for subsurface flow (see Spanoudaki et al. (2009); Yuan et al. (2011); Lou et al. (2018)). As discussed in the previous sub-item, this sophistication level defines the processes that the models can capture, but it brings the trade-off between accuracy and application efficiency in practical cases. On this point, it is essential to assume simplifications in the equation to preserve this trade-off. For surface flow, models can adopt approximations such as diffusive wave or the depth integrate shallow water equations (e.g. Panday e Huyakorn (2004); Gunduz e Aral (2005); Kollet e Maxwell (2006); Wu et al. (2021). In the subsurface flow case, the 3D Richards equations can be simplified to the 2D Boussinesq equations assuming Dupuit-Foreheimer's assumptions are valid.

An essential step in coupled models choosing or developing is to understand the equation simplifications influence on the phenomenons that must be captured in the

modeling process. For example, for coastal environments (e.g., rivers flowing into the sea, estuaries, tidal coastal lagoons), a surface approximation using a diffusive wave model is not applicable, as the absence of the inertial parcel hinders the capture of tidal and incident wave effects (Huang e Yeh, 2009; Kong et al., 2010; Yuan et al., 2011). In subsurface flows, Dupuit-Foreheimer's assumptions can be suitable when the domain's horizontal dimensions are predominant in scale compared to the subsurface layer's vertical dimension (Yuan et al., 2008; Casulli, 2015; Chen et al., 2020). In these assumptions, the hydrostatic approximation is assumed to be valid and the pressure can be expressed in terms of the free-surface elevation (or piezometric head), thus, both flows share the same pressure. Nevertheless, Dupuit-Foreheimer's assumptions can bring inaccurate predictions of the water table at aquifer borders where the vertical component of the flow may have more influence (Marino e Luthin, 1982).

1.4 IPH-ECO Model

The IPH-ECO is a hydrodynamic and ecological model developed to describe the main hydrodynamic, biotic, and abiotic components of continental aquatic ecosystems (e.g., rivers, lakes, estuaries, and reservoirs) in subtropical and tropical environments (Fragoso Jr et al., 2009). The model has been under constant development as a result of the work of Grupo de Pesquisa Ecotecnologia e Limnologia Ambiental/Instituto de Pesquisas Hidráulicas (Fragoso Jr et al., 2009; Pereira, 2010; Pereira et al., 2013b; Cavalcanti et al., 2015, 2016; Cunha et al., 2019, 2020), and its potentiality is reflected in the success of several studies conducted in different locations (Fragoso Jr et al., 2009, 2011; Pereira et al., 2013a; Cavalcanti et al., 2016; de Brito Jr et al., 2018; Munar et al., 2018, 2019).

The IPH-ECO hydrodynamics module solves the 3D Navier-Stokes Equations to describe free surface flows in an unstructured rectangular or triangular grid. It uses a semi-implicit hybrid discretization of finite differences and finite volumes to solve the equations system formed by Navier-Stokes and mass conservation equations (Casulli e Cheng, 1992; Casulli e Cattani, 1994; Casulli e Walters, 2000; Casulli, 2009). The ecological module is an adaptation of the PCLake (Janse, 2005) for subtropical and tropical regimes and gives it the main chemical and biological interactions, ecological processes, and state variables. Both modules are integrated by the solution of the 3D advective-diffusive-reactive transport equation for each constituent. The transport equation solution uses a finite-volume approach optimized with a conservative Local time-stepping algorithm (Cavalcanti et al., 2015) with flux-limiting schemes to enhance its accuracy (Cunha et al., 2019).

1.5 Objectives

1.5.1 General objective

Given the relevance of the interaction between subsurface-surface flows for lakes ecosystem dynamics, the objective of the present study was to propose a numerical adaptation for the hydrodynamic module of the IPH-ECO model to allow the simulation of coupled subsurface-surface flows.

1.5.2 Specifics objectives

- To propose a new approach in the hydrodynamic module of the IPH-ECO model to allow the integration between surface and subsurface flows practically and accurately;
- Validate the new approach against consolidating benchmarks in the literature that represent processes that must be captured by coupled flow models for subtropical lake environments.

1.6 Work organization

This study is formed into four chapters. In the first chapter, the contextualization of the work is performed, presenting its relevance and objectives. In the second one, the governing equations and the proposed numerical scheme are presented and discussed. This chapter also shows the benchmarks used to validate the algorithm. The third chapter shows the validation process of the algorithm. In this step, the simulation results of the benchmarks are compared with similar models and analytical results. Also, a discussion of the limitations encountered at this stage is carried out. The last chapter presents the general conclusion of the work and suggestions for the next steps.

Chapter 2

Methods

In this chapter, the new numerical approximation adopted in the hydrodynamic module of the IPH-ECO model is explained. The numerical scheme adopted is a hybrid semi-implicit finite difference method for the momentum equations with a finite volume method for the conservation equation (a generalized Richard equation) for an unstructured orthogonal grid. This approach is quite similar to the numerical scheme adopted by Kong et al. (2010) and Casulli (2015). Compared to Kong's and Casulli's methods, one of the most important differences is the high-order Lagrangian method used, while the first one uses a linear form and the last one uses a conservative. Furthermore, Casulli's method adopts a sub-grid resolution, while the approach adopted here is only suitable for a coarse grid resolution.

In following sections, the governing equations for the surface and subsurface flows and the numerical solution adopted are explained. Subsequently, the algorithm is summarized, and a set of benchmarks for its validation are presented.

2.1 Assumptions and Governing Equations

The superficial flow is defined by the Reynolds Averaged Navier–Stokes Equations (RANS) and the subsuperficial is defined by Richard's Equation and Darcy's law. The vertical domain is limited below by an impermeable layer (e.g. impervious bedrock) and above by the free surface. Also, it is assumed that a hydrostatic pressure approximation (Dupuit's assumption) is valid (Bear e Verruijt, 2012). Thus, the pressure can be conveniently expressed in terms of the free surface and the piezometric head, and both superficial and subsurface flows share the same pressure (Casulli, 2015).

Considering that the impervious bed and soil layers are known for $\forall(x, y)$ on horizontal domain Ω, the impervious level is located at $z = -h(x, y)$ and soil level at $z = -s(x, y)$ (Figure 2.1), respecting the condition that $-h(x, y) \leq s(x, y)$. The region between that both levels define the permeable layer where subsurface flows occurs. Hence, in cases that $-h(x, y) = -s(x, y)$ for $(x, y) \in \Omega$, the subsurface layer is neglected and only superficial flow occurs.

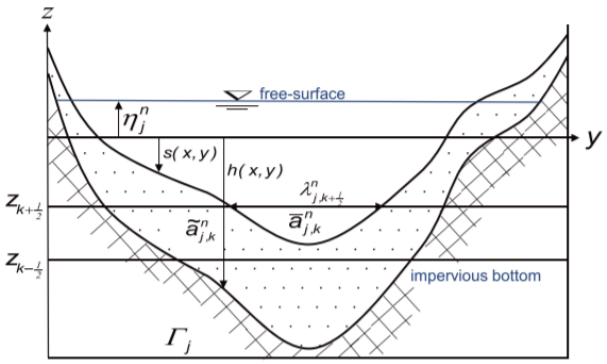

Figure 2.1 – Vertical cross section. Source: (Casulli, 2015).

2.1.1 Superficial Governing Equations

The momentum equations for an incompressible fluid within a Cartesian coordinates system (x, y, z) can be written in the following form:

$$u_t + (V.\vec{\nabla})u - fv = -Pa_x - g\eta_x - gq_x + (\nu^h\ u_x\ )_x + (\nu^h\ u_y\ )_y + \nu^v\ (u_z\ )_z, \tag{2.1}$$

$$v_t + (V.\vec{\nabla})v - fu = -Pa_y - g\eta_y - gq_y + (\nu^h\ v_x\ )_x + (\nu^h\ v_y\ )_y + \nu^v\ (v_z\ )_z, \tag{2.2}$$

$$w_t + \left(\vec{V}.\ \nabla\right) w = -gq_z + \left(\nu^h w_x\right)_x + \left(\nu^h w_y\right)_y + \nu^v\ (w_z)_z \tag{2.3}$$

where $u(x, y, z, t)$, $v(x, y, z, t)$, and $w(x, y, z, t)$ are the velocity components in the horizontal (x and y) and vertical (z) directions, respectively, from velocity vector $V(x, y, z, t)$;nd ∇_{xy} is the gradient operator; ν^h e ν^v are the horizontal and vertical turbulent eddy viscosity coefficients, respectively; t is the time; η is the free-surface elevation from a water-level reference; $p_a(x, y, z, t)$ is the atmospheric pressure; the second term on the right-hand side of Equations (2.1) and (2.2) represent the barotropic contribution to the hydrostatic pressure; $q(x, y, z, t)$ denotes the nonhydrostatic pressure component; f is the Coriolis parameter; and g is the gravitational acceleration.

When a simple hydrostatic approach is considered, Equation (2.3) is neglected and q is assumed to be equal to zero in Equations (2.1) and (2.2). In this case, it is assumed

that the vertical acceleration does not have a significant effect on the velocity field in comparison with the horizontal acceleration, which is the assumption usually applied in simulations of shallow waters (e.g. Jin e Ji 2005; Cavalcanti et al. 2016; Tang et al. 2017; Munar et al. 2018).

The volume conservation is expressed by the incompressibility condition and the continuity equation, given by:

$$\vec{\nabla}.\vec{V} = u_x + v_y + w_z = 0. \tag{2.4}$$

At the domain boundaries, the "free-slip" boundary condition was implemented. Also, the Dirichlet and Neumann conditions were assigned to represent the normal and tangential velocities in the solid boundaries, respectively.

The tangential stress boundary conditions for the momentum equations (Equations 2.1 and 2.2) are specified at the free-surface by the prescribed wind stresses, which can be approximated as:

$$\nu^v u_z = \gamma_t \left(u_a - u\right), \ \nu^v v_z = \gamma_t \left(v_a - v\right), \quad at \quad z = \eta, \tag{2.5}$$

where u_a and v_a are the horizontal wind velocity components, and γ_T is a non-negative wind stress coefficient. The bottom friction is specified by:

$$\nu^v u_z = \gamma_B u^*, \ \nu^v v_z = \gamma_B v^*, \quad at \quad z = -s, \tag{2.6}$$

where γ_B is a non-negative bottom friction coefficient; $u*$ and $v*$ are the horizontal superficial velocity component tangential at the sediment-water interface.

2.1.2 Subsuperficial Governing Equations

The governing equation to subsurface flow velocities is based on Darcy's theory given by:

$$V^g \ = \ -\mathcal{K}.\nabla_h \eta \tag{2.7}$$

where $K(x, y)$ is the non-negative hydraulic conductivity; $V^g(x, y, z, t)$ is the subsurface velocity vector; and ∇_{xy}, here, is the horizontal gradient operator. As in regional scales environmental flows are commonly characterized by a much larger horizontal extent than the vertical scales, the vertical velocity component is neglected and a two-dimensional approach is adopted for subsurface flow. The horizontal velocities in the subsurface region are given by two-dimensional Darcy's Law:

$$u^g = -\mathcal{K}\frac{\partial \eta}{\partial x}, \tag{2.8}$$

and

$$v^g = -\mathcal{K}\frac{\partial \eta}{\partial y}. \tag{2.9}$$

where $\mathcal{K}(x, y)$ is the non-negative hydraulic conductivity.

The continuity equation governing the subsurface flow is based on Richard's equation for porous media, given by:

$$\frac{\partial \theta}{\partial t} + \nabla . V^g = 0 \tag{2.10}$$

where $\Theta(x, y, z, t) = \epsilon(x, y, z)S(x, y, z)$ is the moisture content, which $\epsilon(x, y, z)$ is the soil porosity and $S(x, y, z)$ is the water saturation. When the subsurface layer becomes saturated, the first term vanishes and Equation 2.10becomes similar to the incompressibility condition give by Equation 2.4 to surface flow. In our approach, we used Darcy's constitutive relationship model to describe the water saturation, which can be defined by the Heaviside step function ($\mathcal{H}$) as $S(x, y, z) = \mathcal{H}(\eta - z)$.

2.1.3 The integrated mass conservation equation and boundaries conditions

To generalize the algorithm to obtain a relationship that assures the mass conservation in the common interfaces between coupled flows, the saturation and porosity functions are prolonged to the superficial domain. A virtual porosity in the superficial layer was setting like $\epsilon(x, y, z) = \mathcal{H}(\eta - z)$, which implies that $\epsilon(x, y, z) = 1$ when the superficial layer is wet and $\epsilon(x, y, z) = 0$, otherwise. Thus, the kinematic condition at free-surface now is defined by:

$$\epsilon^s \eta_t + u^s \eta_x + v^s \eta_y = w^s, \tag{2.11}$$

where $\eta = \eta(x, y, t)$ represents the free-surface elevation; $\epsilon^s = \epsilon(x, y, \eta)$ is the porosity at free-surface; $u^s = u(x, y, \eta)$, $v^s = v(x, y, \eta)$ and $w^s = w(x, y, \eta)$ are the velocity components in free-surface.

At the impervious bottom, the kinematic condition states that the perpendicular component velocity must vanish, and is given by:

$$u^b h_x + v^b h_y + w^b = 0, \tag{2.12}$$

where $h = h(x, y, t)$ represents the bottom profile elevation; $u^b = u(x, y, -h)$, $v^b = u(x, y, -h)$ and $w^b = u(x, y, -h)$ are the velocity components at the bottom.

Now, considering the kinematics conditions aforementioned, and the generalized porosity function, the integration of the Equation 2.10 over the depth yields the following free-surface equation:

$$\frac{\partial}{\partial t}\left(\int_{-h}^{\eta} \epsilon dz\right) + \frac{\partial}{\partial x}\left(\int_{-h}^{\eta} u dz\right) + \frac{\partial}{\partial y}\left(\int_{-h}^{\eta} v dz\right) = 0. \tag{2.13}$$

Equation (2.13) represents the exact mass balance in the entire water column for all (x, y) in the domain Ω and any time $t > 0$. When including both the surface and subsurface horizontal fluxes, this condition assures the normal flow continuity between the surface and subsurface flow regions.

2.2 Numerical discretization

2.2.1 Computational Grid and Flow Variables

The computational grid can be described as a generic unstructured orthogonal grid, covered by non-overlapping convex polygons Ω_i, $i = 1, 2, \ldots, N_p$ (Figure 2.2), with area P_i and N_s sides Γ_j with length λ_j. When the cell is wet the λ_j represents the wet length $\lambda^n_{j,k+\frac{1}{2}}$. The nonzero distance between centers of two adjacent polygons which share the $j-th$ side is denoted with δ_j. The two polygons which share the Γ_j face of the grid are identified by the indices $l_{(j)}$ and $r_{(j)}$. Also, $\wp_{(i,j)}$ denotes the neighbor of polygon $i-th$ that share side j.

Along the vertical direction a simple finite difference discretization, not necessarily uniform, is adopted. The spatial discretization consists of elements whose horizontal faces are the polygon of a given orthogonal grid, represented by the layers at $k+\frac{1}{2}$ (upper face) or $k-\frac{1}{2}$ (bottom face), whose height, for each layer, is Δz_k (Figure 2.1). By denoting with $\Delta z_{k+\frac{1}{2}}$ a given top computational cell level surface, the vertical discretization step is defined by $\Delta z_k = \Delta z_{k+\frac{1}{2}} - \Delta z_{k-\frac{1}{2}} \quad k = 1, 2, \ldots, N_s$. The water surface elevation (η^n_i) at time t_n, is located at the barycenter of the upper horizontal face for each $i-th$ element.

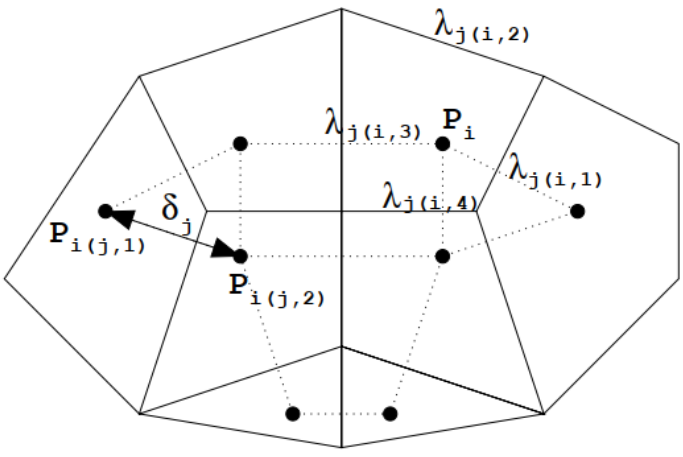

Figure 2.2 – Discrete flow variables on structured grid. Source: Casulli (2009).

The total wet area of each vertical face is defined by $a^n_{j,k} = \bar{a}^n_{j,k} + \tilde{a}^n_{j,k}$, such that $\bar{a}^n_{j,k}$ and $\tilde{a}^n_{j,k}$ are the non-negatives surface and subsurface wet areas for each vertical face, respectively. The first one is given by $\bar{a}^n_{j,k} = \lambda_j \Delta \bar{z}^n_{j,k},$, where $\Delta \bar{z}^n_{j,k}$ is the surface

wetted vertical distance Δz_k. Where, for this case the $\Delta \bar{z}^n_{j,k}$ is defining by $\Delta \bar{z}^n_{j,k} = max\left[0, min\left(z_{k+\frac{1}{2}}, \eta^n_j\right) - max\left(z_{k-\frac{1}{2}}, -s\right)\right]$.

While, the non-negative subsurface wet area of each vertical face is similarly defined by $\tilde{a}^n_{j,k} = \lambda_j \tilde{z}^n_{j,k}$, where $\Delta \tilde{z}^n_{j,k}$ is the subsurface wetted vertical distance. In this case, the $\Delta \tilde{z}^n_{j,k}$ is defining by $\Delta \tilde{z}^n_{j,k} = max\left[0, min\left(z_{k+\frac{1}{2}}, \eta^n_j, -s\right) - max\left(z_{k-\frac{1}{2}}, -h\right)\right]$.

The surface and subsurface horizontal velocity components are assumed constant over the vertical face of each computational cell, being set at the center of each cell. The horizontal averaged velocity components in each wet vertical faces are described as:

$$u^n_{j,k} = \frac{\bar{a}^n_{j,k}\bar{u}^n_{j,k} + \tilde{a}^n_{j,k}\tilde{u}^n_{j,k}}{a^n_{j,k}}, \tag{2.14}$$

where the positive direction from each horizontal velocity component is chosen to go from $l_{(j)}$ to $r_{(j)}$. Furthermore, for each wetted cell, The averaged normal velocity in each horizontal face is defined by $w^n_{j,k+\frac{1}{2}}$.

2.2.2 Numerical Approximation

For the momentum equations (Equations 2.1 and 2.2), a semi-implicit finite-difference method was applied for each face Γ_j as follow:

$$\bar{a}^n_{j,k}\bar{u}^{n+1}_{j,k} = \bar{a}^n_{j,k}F\bar{u}^n_{j,k} - g\Delta t\bar{a}^n_{j,k}\frac{\eta^{n+\theta}_{r(j)} - \eta^{n+\theta}_{l(j)}}{\delta_j} - \Delta t\gamma^n_{j,k}\bar{u}^n_{j,k} +$$
$$\Delta t\left\{\lambda^n_{j,k+\frac{1}{2}}\nu^n_{j,k+\frac{1}{2}}\frac{\bar{u}^{n+1}_{j,k+1} - \bar{u}^{n+1}_{j,k}}{\Delta z_{k+\frac{1}{2}}} - \lambda^n_{j,k-\frac{1}{2}}\nu^n_{j,k-\frac{1}{2}}\frac{\bar{u}^{n+1}_{j,k} - \bar{u}^{n+1}_{j,k-1}}{\Delta z_{k-\frac{1}{2}}}\right\}, \quad k = \bar{m}_j, \bar{m}_j{+}1, \ldots, \bar{M}_j, \tag{2.15}$$

where F is an explicit finite difference operator, which accounts for the contribution from the discretization of the Coriolis, advection and horizontal friction terms; Δt denotes the time-step; $\eta^{n+\theta} = \theta\eta^{n+1} + (1-\theta)\eta^n$ and $\theta \,\epsilon\, [\frac{1}{2}, 1]$ is implicitness parameter from θ-method (Casulli, 1990) ; $\gamma^n_{j,k}$ is the friction coefficient associated with the boundaries conditions Equations 2.5 and 2.6; $\bar{m}_j$ and $\bar{M}_j$ are the lowest and the highest superficial wet vertical face, respectively. Note that the value of $\bar{M}_j$ may change at each time level t_n, since the free surface change on their spatial distribution j.

For the explicit finite difference operator F, the Eularian-Lagragian discretization (Casulli e Cheng, 1992; Casulli e Walters, 2000) was adopted, and it is given as follows:

$$F\bar{u}^n_{j,k} = \frac{\left[1 - \theta(1-\theta)f^2\Delta t^2)\right]u^*_{j,k} + f\Delta t v^*_{j,k}}{1 + \theta^2 f^2 \Delta t^2} + \Delta t\nu^h \triangle_h u^*_{j,k}, \tag{2.16}$$

where $u^*_{j,k}$ denotes the velocity component normal to the $j-th$ side of the grid and $v^*_{j,k}$ is the tangential velocity component in a right-hand coordinate system. The Lagrangian trajectory is approximated by integrating the velocity backwards in time from node (j,k) at $t^n + 1$ to its location at time t^n, which is done by a Multi-Step Euler approach. Then, both components are interpolated at of the Lagrangian trajectory based on the values at adjacent grid points using a quadratic interpolation method similar to that adopted by Hodges et al. (2000).

The Equation 2.15 application over the computational domain, provides a set of N_s independent linear tridiagonal systems of at most N_z equations. In vectorial notation, Equation (2.15) becomes:

$$\mathbf{A_j^n \bar{u}_j^{n+1}} = \mathbf{G_j^n} - g\theta\Delta t \frac{\eta^{n+1}_{r(j)} - \eta^{n+1}_{l(j)}}{\delta_j} \mathbf{\bar{a}_j^n}, \tag{2.17}$$

where $\boldsymbol{A_j^n}$, is a symmetric, positive definite, tridiagonal matrix that includes bottom friction and vertical viscosity terms; $\mathbf{\bar{u}_j^{n+1}}$ are vectors containing the unknown surface velocities; $\mathbf{\bar{a}_j^n}$ are vectors whose entries are the wet superficial vertical face area; and $\mathbf{G_j^n}$ is a vector containing the known explicit terms in Equation 2.15.

For subsurface flow region, the Darcy's Equations are discretized in a simple non-dependent time implicit finite difference approximation:

$$\tilde{u}^{n+1}_{j,k} = -\mathcal{K}_{j,k} \frac{\eta^{n+1}_{r(j)} - \eta^{n+1}_{l(j)}}{\delta_j}, \quad k = \tilde{m}_j, \tilde{m}_j + 1, \ldots, \tilde{M}_j, \tag{2.18}$$

where $K_{j,k}$ is the face averaged hydraulic conductivity; $\tilde{m}_j$ and $\tilde{M}_j$ are the lowest and the highest subsurface wet vertical face, respectively. Once we adopted Darcy's constitutive relationship model to define soil saturation, the $\tilde{M}_j$ values change spatially over each time level t_n to take into account free-surface changes, likewise, the surface flow discretization.

The application of Equation 2.18 produces a set of $N_s N_z$ explicit equations for the horizontal subsurface velocities components, which in the vectorial form can be written as:

$$\mathbf{\tilde{u}_j^{n+1}} = -\mathcal{K}_\mathbf{j} \frac{\eta^{n+1}_{r(j)} - \eta^{n+1}_{l(j)}}{\delta_j}, \tag{2.19}$$

where $\mathbf{\tilde{u}_j^{n+1}}$ are vectors containing the unknown subsurface velocities; and $\mathbf{K_j}$ are the prescribed non-negative hydraulic conductivity vectors.

For the free-surface equation (Equation 2.13), a semi-implicit finite volume approx-

imation was applied to obtain the following volume expression to i-th polygon:

$$V\left(\eta_i^{n+1}\right) = V\left(\eta_i^n\right) + \Delta t \sum_{j \epsilon S_i} \sigma_{i,j} \left(\sum_{j=\bar{m}_j}^{\bar{M}_j} \bar{a}_{j,k}^n \bar{u}_{j,k}^{n+\theta} + \sum_{j=\tilde{m}_j}^{\tilde{M}_j} \tilde{a}_{j,k}^n \tilde{u}_{j,k}^{n+\theta} \right), \tag{2.20}$$

where $\bar{u}_{j,k}^{n+\theta} = \theta \bar{u}_{j,k}^{n+1} + (1-\theta)\bar{u}_{j,k}^{n+1}$ and $\tilde{u}_{j,k}^{n+\theta} = \theta \tilde{u}_{j,k}^{n+1} + (1-\theta)\tilde{u}_{j,k}^{n+1}$; and $V\left(\eta_i^{n+1}\right)$ is a non-negative and non-decreasing function that describe the water volume in i-th column, for a given η_i^{n+1}, given as:

$$V\left(\eta_i^{n+1}\right) = \int_{\Omega_i} \left[\int_{-\infty}^{\eta_i^{n+1}} \epsilon(x,y,z) dz \right] d\Omega_i; \tag{2.21}$$

and $\sigma_{i,j}$ is a sign function associated with the orientation of the normal velocities defined on the j-th vertical faces, described by:

$$\sigma_{i,j} = \frac{r(j) - 2i + l(j)}{r(j) - l(j)}, \tag{2.22}$$

where to $\sigma_{i,j} = 1$, a positive velocity on the j-th side corresponds to outflow, and if $\sigma_{i,j} = -1$, a positive velocity on the j-th side corresponds to inflow to the i-th water column.

When applied on all computational domain, Equation 2.20 yields a mildly nonlinear system of N_p equations for η_i^{n+1}. Substituting Equations 2.17 and 2.19 in Equation 2.22 yields the following discrete free-surface equation in vetorial form:

$$V\left(\eta_i^{n+1}\right) - \theta \Delta t \sum_{j \epsilon S_i} \left\{ \left[g\theta\Delta t (\bar{\mathbf{a}}^{\mathbf{T}} \mathbf{A}^{-\mathbf{1}} \bar{\mathbf{a}})_{\mathbf{j}}^{\mathbf{n}} + (\tilde{\mathbf{a}}^{\mathbf{T}} \mathcal{K})_{\mathbf{j}}^{\mathbf{n}} \right] \frac{\eta_{\wp(i,j)}^{n+1} - \eta_i^{n+1}}{\delta_j} \right\} =$$

$$V\left(\eta_i^n\right) - \Delta t \sum_{j \epsilon S_i} \sigma_{i,j} \left[(1-\theta)(\bar{\mathbf{a}}^{\mathbf{T}} \bar{\mathbf{u}} + \bar{\mathbf{a}}^{\mathbf{T}} \tilde{\mathbf{u}})_{\mathbf{j}}^{\mathbf{n}} + \theta (\tilde{\mathbf{a}}^{\mathbf{T}} \mathbf{A}^{-\mathbf{1}} \mathbf{G})_{\mathbf{j}}^{\mathbf{n}} \right]. \tag{2.23}$$

The mildly nonlinear equations system defined by Equation 2.23 is solved every time step with a Newton Method. Thus, once the free-surface has been determined, Equation 2.17 becomes a set of linear systems that can be solved straightforwardly by a linear system solver algorithm (here, was chosen the Thomas' Method) to obtain the velocity components $\bar{u}_{j,k}^{n+1}$. Furthermore, the subsurface velocities components $\tilde{u}_{j,k}^{n+1}$ are directly obtained from Equation 2.19.

Finally, the averaged normal velocity in each horizontal face is achieved by applying a finite volume form of the incompressibility condition (Equation 2.4), as follow:

$$\left(\sum_{j\epsilon S_i}\sigma_{i,j}a^n_{j,k}u^{n+1}_{j,k}\right)+a^n_{j,k+\frac{1}{2}}w^{n+1}_{j,k+\frac{1}{2}}-a^n_{j,k-\frac{1}{2}}w^{n+1}_{j,k-\frac{1}{2}}=0,\quad k=m_i,m_i^n+1,\ldots,M_i^n-1, \tag{2.24}$$

where $a^n_{j,k}$ and $a^n_{j,k\pm\frac{1}{2}}$ are the total wet areas; $u^{n+1}_{j,k}$ and $w^{n+1}_{j,k\pm\frac{1}{2}}$ are the corresponding face averaged velocities in time level t_{n+1}; m_i and M_i denote the lowest and the highest control volume within the $i-th$ water column. Reorganizing Equation 2.24, the vertical velocity component at each time t_n is:

$$w^{n+1}_{j,k+\frac{1}{2}}=\frac{a^n_{j,k-\frac{1}{2}}w^{n+1}_{j,k-\frac{1}{2}}-\sum_{j\epsilon S_i}\sigma_{i,j}a^n_{j,k}u^{n+1}_{j,k}}{a^n_{j,k+\frac{1}{2}}},\quad k=m_i,m_i^n+1,\ldots,M_i^n-1, \tag{2.25}$$

where no flux condition is applied in bottom $w^{n+1}_{j,m-\frac{1}{2}}=0$.

2.2.2.1 Algorithm Summary

In summary, the algorithm take the following steps:

1. Definition of initial parameters, initial conditions, and boundary conditions.
2. The wet areas $\bar{a}$ and $\tilde{a}$ are determined.
3. Solution of convective terms using the Eulerian-Lagrangian Method.
4. The mildly nonlinear system (Equation 2.23) is solved through the Nested-Newton Method (Casulli e Zanolli, 2012) to obtain simultaneously the new water level η_i^{n+1} and corresponding columnar fluid volumes $V\left(\eta_i^{n+1}\right)$.
5. The new horizontal surface velocities $\bar{\mathbf{u}}_\mathbf{j}^{\mathbf{n+1}}$ are obtained as solution of the N_s linear tridiagonal systems (Equation 2.17).
6. The new horizontal subsurface velocities $\tilde{\mathbf{u}}_\mathbf{j}^{\mathbf{n+1}}$ are obtained through Equation 2.19.
7. Next, the new vertical velocities $w^{n+1}_{j,k+\frac{1}{2}}$ are determined from the recursive relation defined by Equation 2.25.

2.2.2.2 Numerical Method Remarkables

The numerical analysis by Casulli e Cattani (1994) on the method formed by Equations 2.15 and 2.24 shows that its stability is independent of celerity, friction and vertical viscosity. Its stability will be associated with the implicitness factor choice θ, which

had to be chosen between $1/2 \leq \theta \leq 1$, the discretization of the horizontal viscosity, and the choice of the operator F. Note that, if the horizontal viscosity is neglected, and the parameter theta and a stable operator F are chosen appropriately, the method becomes unconditionally stable for any time step.

The stability, accuracy, and numerical diffusion associated with the Eulerian-Lagrangian operator will depend on the interpolation method adopted (Casulli, 1990). Here, a high-order interpolation method was adopted. High-order interpolation methods may reduce numerical diffusion but may introduce spurious oscillations. Nevertheless, as the interpolation adopted here has been tested and validated by Cunha et al. (2019), exhibiting excellent results in avoiding diffusion, it has been kept.

The approach adopted for the domain discretization and the numerical scheme allows the IPH-ECO Model to be applied directly to simulations where a coupled surface-subsurface or just a surface flow is simulated. When a sediment layer $s(x, y)$ and an impermeable layer $h(x, y)$ is prescribed, the algorithm will automatically allow coupled flow (soil parameters must also be entered by the user, or the default settings will be retained). If only one sediment layer $s(x, y)$ is prescribed, the algorithm considers this layer to be an impermeable bathymetry, setting $h(x, y) = s(x, y)$, and only surface flow is allowed. This same principle can be partially applied in regions where the sediment layer would intersect the impermeable layer.

2.2.3 Numerical Experiments

The numerical approach presented in the previous items was implemented in the source code of the hydrodynamic module IPH-ECO. This version of the IPH-ECO model was then tested against consolidated benchmarks used for verification and validation of numerical flow methods.In the first case, the bathymetry is set equal to the impermeable bottom and Dupuit's assumption is validated. The second tests the model's capability to simulate the transfer of tidal effect through a permeable sand bar. Finally, the third case is used to validate the superficial and the coupled subsurface-surface flow in a catchment. The numerical experiments are described below.

2.2.3.1 Flow-through a porous dam

In this benchmark, a steady-state flow through a vertical porous dam was assessed. The water levels on both sides of the dam are set with different and constant values so that a permanent hydraulic head gradient is achieved. The dam has a length and a height equal to 10 m (Figure 2.3). The simulation results were compared with the analytical solution of flow through the porous medium defined by Dupuit's Parabola Equation, which

is defined as follows:

$$\eta(x) = \left[H_1^2 - \frac{x}{L}(H_1^2 - H_2^2)\right]^{\frac{1}{2}}, \tag{2.26}$$

where H_1 and H_2 can be defined as the constant water levels at the left and right side of the dam, respectively; and L is the dam's length.

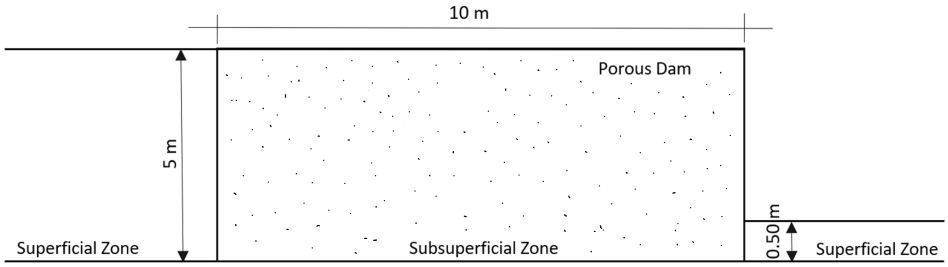

Figure 2.3 – Domain dimensions for the flow-through porous dam numerical experiment.

Also, the simulation was carried out with two subsurface parameter settings to illustrate the flow's independence of soil parameters for this test case. This is an important assumption to assess, once that Dupuit's Equation depends just on the hydraulic gradient defined by the boundary condition (Equation 2.26).

The water level on the left and right sides of the dam was prescribed equally at 5 m and 0.5 m, respectively, and was kept constant over the whole simulation. Also, a no-flow condition was prescribed everywhere else. The initial water level in the subsurface zone was prescribed as $\eta(x, 0) = 5 - 0.45x$. Thus, the simulation was performed by the steady-state is reached with a step size of $\Delta t = 3600$s.

2.2.3.2 Flow in a tidal lagoon

This benchmark is based on a laboratory experiment conducted by Ebrahimi et al. (2007). In this experiment, a lagoon was separated from a tidal open sea area by a permeable sand bar. It represents the exchange between the idealized tidal basin and the adjacent lagoon, which has made it a classic numerical experiment in verifying and validating the models' ability to simulating coupled flows between these areas (Liang et al., 2007; Yuan et al., 2008, 2012; Kong et al., 2010; Casulli, 2015, 2017; Shokri et al., 2018; Chen et al., 2020).

The numerical domain is described in Figure 2.4), where the points A, B and C shows the local where water elevation and velocities were collected in Ebrahimi et al. (2007)'s experiment. The permeable sand bar was characterized by an porosity $\epsilon = 0.3$ and hydraulic conductivity $\mathcal{K} = 1.0$ cm/s. For the superficial flow, the horizontal viscosity was neglected and the Chezy's bed roughness was set equal to 50 m/s.

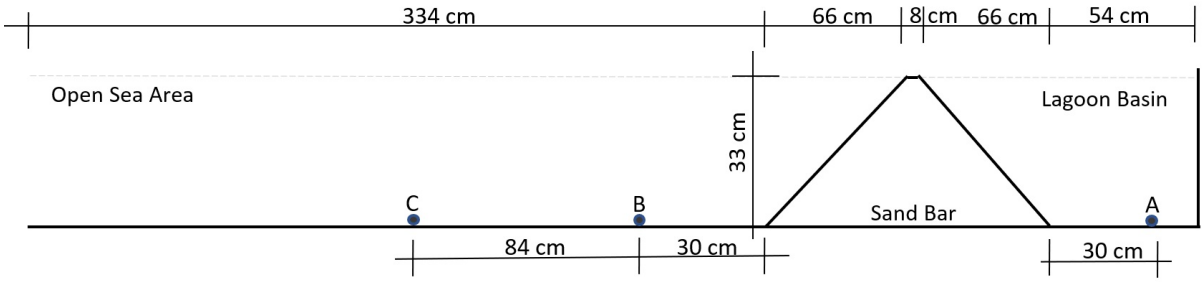

Figure 2.4 – Domain dimensions for the tidal lagoon numerical experiment.

In the whole domain a no-flow boundary condition was set, except at the left boundary in the open sea area, where a harmonic boundary condition (simulating tidal effect) was applied. The harmonic boundary condition oscillates with a constant amplitude of $a = 6$ cm, a period of T= $355s$, and a mean water level of 21.4 cm, which can be defined by $\eta(0,t) = 21.4 + acos\left(\frac{2\pi t}{T}\right)$.

At the initial time ($t = 0$) the water level was prescribed to be 27.4 cm and the velocities were set equal to zero in the whole domain. The simulation was carried out by 10 tidal cycles with a time-step equal to $\Delta t = 5$ s and numerical parameters was set $\Delta x = 2$ cm and $\theta = 0.62$.

2.2.3.3 Overland flow in a V-shaped catchment

In this benchmark, the overland flow generated by a rainfall event in a 2D inclined V-shaped catchment is evaluated. This benchmark was first applied by Di Giammarco et al. (1996) and has been used to assess the models' capability to reproduce surface runoff using different sets of equations and numerical approximations (Panday e Huyakorn, 2004; Kollet e Maxwell, 2006; Sulis et al., 2010; Tian e Liu, 2011; Liang et al., 2016). In this version, the catchment superficial layer was considered impermeable. A coupled subsurface flow adaptation was applied to evaluate the soil's infiltration influence on runoff behavior (Panday e Huyakorn, 2004; Casulli, 2015, 2017). Both versions were applied in the present study.

The catchment is composed of two slope planes with a length of 800 m and a width of 1000 m connected by a river channel with a length of 1000 m and 20 m wide (Figure 2.5). The surface slopes are 0.05 perpendicular and 0.02 parallel to the channel. The channel slope is 0.02 in the y-axis direction, equal to the slopes, which maintains its depth constant (set equal to 1 m). Manning's coefficient was set equal to 0.015 $s.m^{-1/3}$ for the slopes and 0.15 $s.m^{-1/3}$ for the channel. The rainfall rate of 10.8 mm/h was applied in the whole domain for 90 min, with a zero rate in the subsequent 90 min of recession. The implicitness factor was set equal $\theta = 0.60$. Also, a constant spatial discretization of $\Delta x = \Delta y = 20$ m and a constant time-step of 5 s was used.

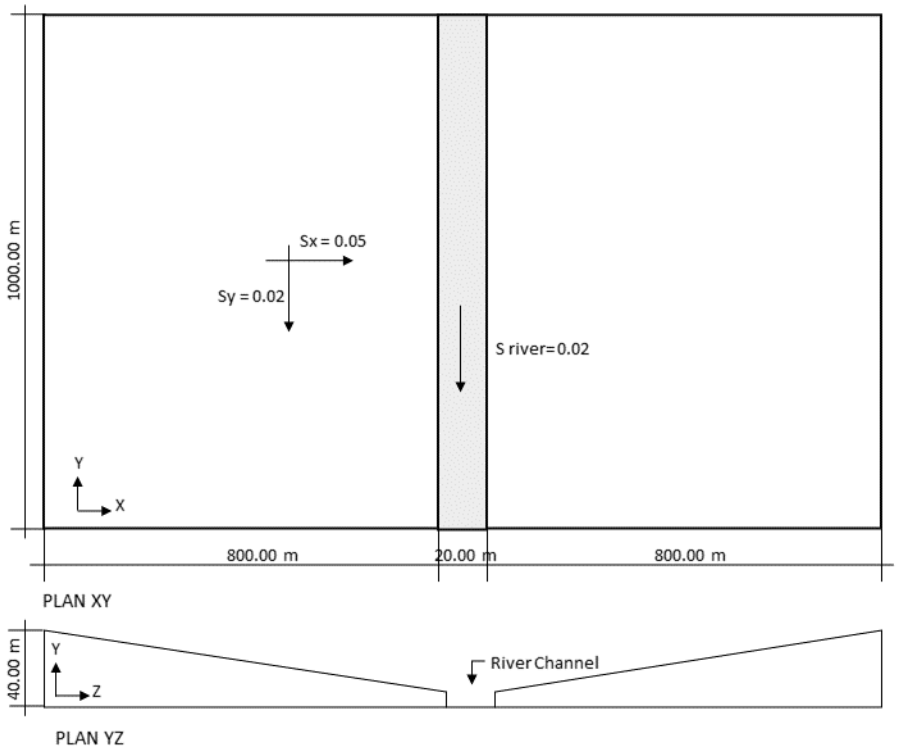

Figure 2.5 – Schematic description of the Tilted V-Catchment.

A no-flow boundary condition was imposed in the whole domain except at the downstream end of the channel, where a critical depth boundary condition was imposed. This boundary condition was imposed to allow compared the results with the Di Giammarco et al. (1996); Panday e Huyakorn (2004)(MODHMS Model) and Parflow models' results.

In the coupled subsurface-surface flow adaptation, the basin surface was considered permeable, and a 20 m layer of sediment was added across the basin from the outlet of the river channel.

Chapter 3

Results and Discussion

3.1 Model Validation

3.1.1 Flow-through a porous dam

The simulated water levels are compared with the analytical water level in Figure 3.1. The model results show good agreement (in both settings the root of the mean square error is 0.001 m). The subsurface water table simulated shown independence from soil parameters and follows Dupuit's parabola as expected. These results were similar to those obtained by the models of Liang et al. (2007),Yuan et al. (2012) and Shokri et al. (2018) for a similar test case.

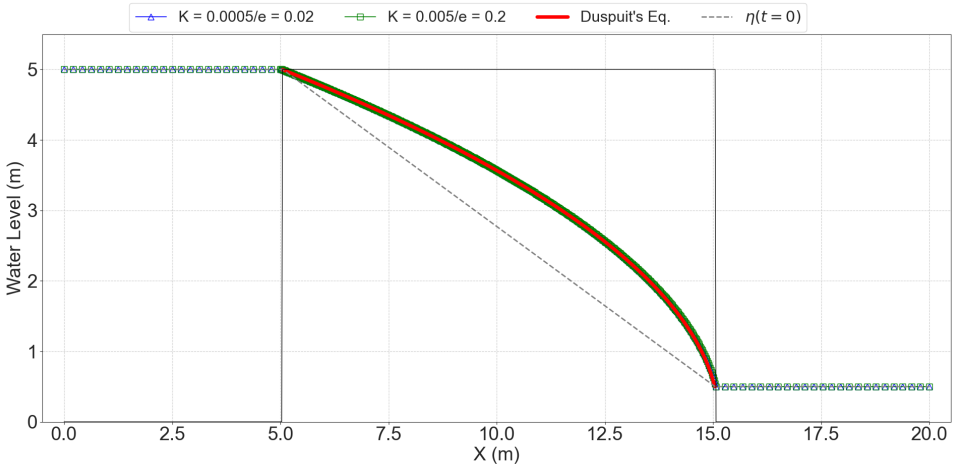

Figure 3.1 – The simulated water levels with a different combination of soil parameters compared to Dupuit's Equation solution for the subsurface zone inside the porous dam.

3.1.2 Flow in a tidal lagoon

In Figure 3.2 the simulated water levels relative to mean water level are compared with the experimental data collected in both the lagoon (point A) and the open sea area (point B) (Figure 2.4). The numerical results show good agreement with the laboratory data, well simulate the observed damping and phase shift of the tidal oscillations (near 90° between lagoon e open sea area water levels). Additionally, in Figure 3.3 the velocity simulated for the last three tidal cycles at point C is compared with the experimental data and shows good results as well. All the results found also in good agreement with results computed previously by other similar models (Liang et al., 2007; Kong et al., 2010; Casulli, 2015; Shokri et al., 2018; Chen et al., 2020).

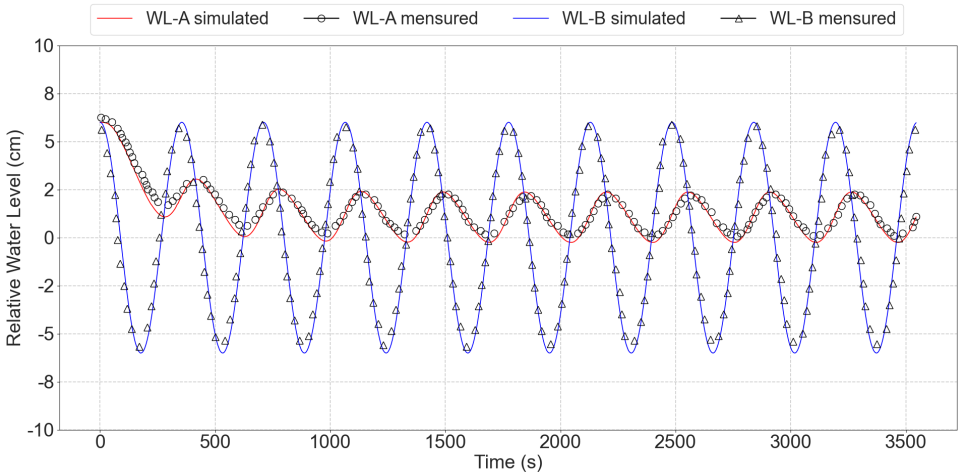

Figure 3.2 – Verification of water surface levels at points A and B.

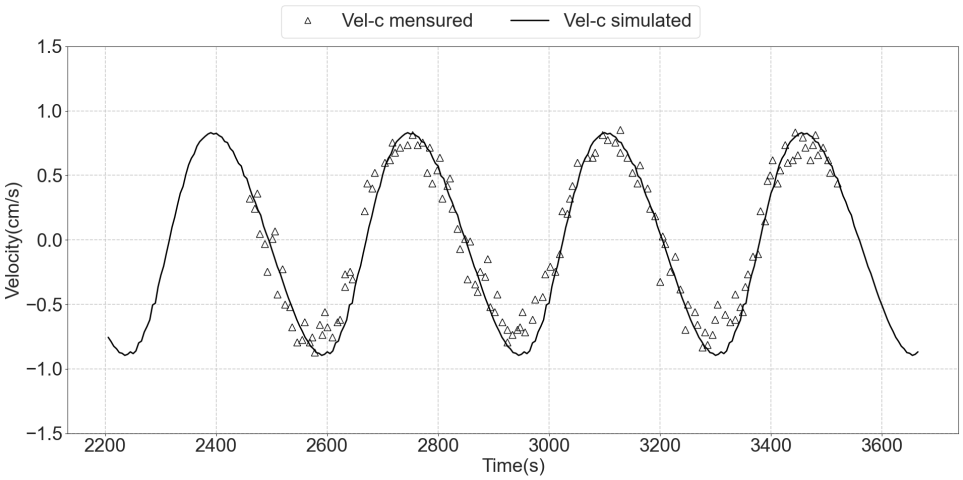

Figure 3.3 – Verification of water surface velocity at point C.

In Figure 3.4 the simulated water levels at low and high tide conditions are compared against the results obtained by the Casulli (2015) and Chen et al. (2020) models. For the low tide condition, the model result was very similar to the Casulli model and showed a

slight difference compared to the Chen model. In the high tide condition, a similar effect occurs in the open sea zone, while in the lagoon zone all models showed a slight difference between each other. In the case of the Chen model, these differences can be attributed to the effect of subgrid resolution on model accuracy. While in the Casulli model there exists the influence of subgrid resolution combined with the utilization of a different Lagrangian operator.

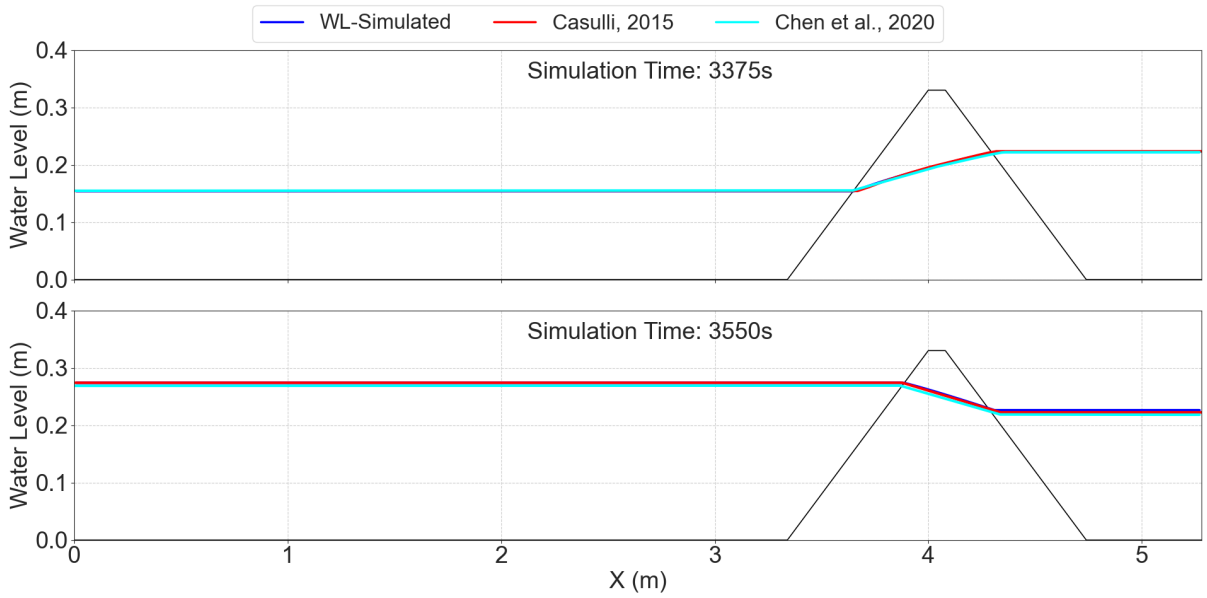

Figure 3.4 – Comparison between simulated water level and previously models' results to water levels at low tide (upper) and at high tide (lower).

To evaluate the step-time effect on the model accuracy, a sensitivity analysis was performed. The model showed similar behavior to the numerical model of Kong et al. (2010). As shown in Figure 3.5, the simulation error increases as the time step become larger. While the results with $\Delta t \leq 5$ s show only slight differences. Thus, it can demonstrate the suitability of choosing the time step $\Delta t = 5$ s for the test case validation. This time step is much larger than the one used by other models (Liang et al., 2007; Yuan et al., 2008, 2012; Shokri et al., 2018) and has also demonstrated good accuracy.

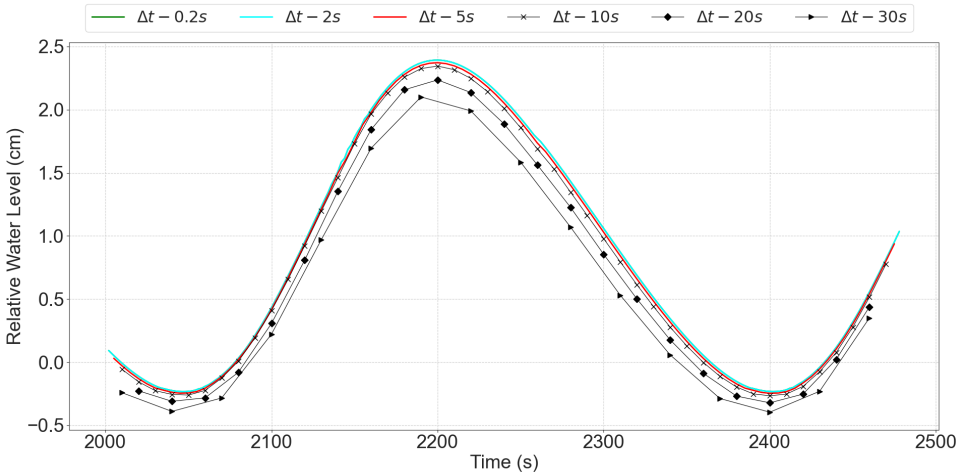

Figure 3.5 – Time-step effect in water level simulation.

3.1.3 Overland Flow in a V-Catchment

Figure 3.6 shows the simulated results against the other model's results. In general, the simulation shows excellent agreement for the peak flow discharge and the receding limb of the hydrograph. The main differences were detected principally in the initial flow rate and the rising limb.

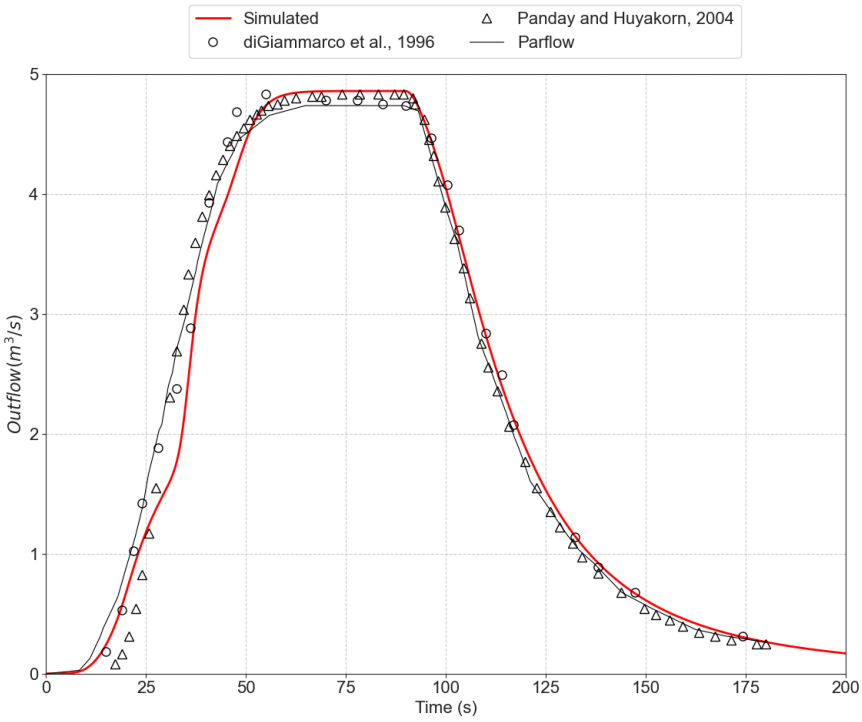

Figure 3.6 – Comparison between simulated outflow against other models.

The differences in the initial flow rate are more evident in the Panday e Huyakorn (2004) model results. It may be associated with the time step used in the simulation. A

constant time step was used in our simulation, similar to the ParFlow model simulation, while in the Panday e Huyakorn (2004) simulation an adaptive time step was applied. In our tests, we performed simulations with different time steps (both larger and smaller than the adopted), and it was evident their effect on the accuracy of the result, especially for capturing the initial transient up to the peak of outflow. Moreover, the principal differences may be associate with the different superficial flow approximations used for each model. In this study, the complete RANS was adopted, while Di Giammarco et al. (1996) uses a diffusive wave approximation, and Panday e Huyakorn (2004) and model Parflow using a kinematic wave approximation. The higher slope in the planes provides a predominance of the gravity terms on the flow, which implies that the kinematic wave and diffusive wave approximation can be suitable. However, neglecting the inertial terms can lead to errors of 5% - 10% (Choi et al., 1993).

The subsurface-surface coupled version of this experiment presented convergence problems, and its results are discussed in the following sub-item.

3.2 Discussion

The results for the first benchmark were quite satisfactory, showing agreement of the algorithm with a particular case of porous media flow with an analytical solution based on Dupuit's assumptions. Despite the simplicity of this benchmark, it is a good approximation to evaluate the water table height and the magnitude of the flows for simulation in a domain where the horizontal scales are significantly less than the vertical and the flows are well developed, especially for the cases where (H1 - H2)/L << 1 (Rehbinder e Wörman, 1994).

For the simulation of the lagoon benchmark under tidal effect, was identified spurious oscillations, which were smoothed by adopting the parameter value $\theta = 0.62$. For this benchmark, the study by Casulli (2015) used $\theta = 0.60$ and in the study by Kong et al. (2010) this parameter was not made explicit. This numerical effect is associated with the use of high-order numerical schemes, as is the case of the quadratic Eulerian-Lagrangian scheme adopted in this study. It is also observed in the study by Shokri et al. (2018), which used a second-order centered upstream scheme in discretizing the advective terms. Numerically increasing the θ value inserts numerical damping into the numerical scheme (Casulli e Cattani, 1994), avoiding the high-frequency noise associated with this numerical phenomenon. In practical terms, this benchmark demonstrates the model's applicability in representing the tidal effect transfer across the coastal region that often limits the encounter between coastal lagoons and the sea. This forcing effect is quite relevant in the nutrient transport and ecological dynamics of these ecosystems (Sophocleous, 2002; Flöder e Burns, 2004; Xin et al., 2011; Ratnayake et al., 2018; de Brito Jr et al., 2018; Jeong e

Kwak, 2020) which makes it critical for the model to capture this effect well.

The v-catchment superficial simulation showed satisfactory results compared to the other models' results. However, when simulating the subsurface-surface coupled flows, the model exhibited convergence problems. The nonlinearity of Equation 2.21 induced convergence problems for Newton's algorithm when the subsurface-surface flow transition process increased in the domain. The main problem arises from that in the transition region between the flows, the derivative of Equation 2.21 changes direction abruptly (Figure 3.7), which makes the linearization process of Newton's algorithm non-conservative.

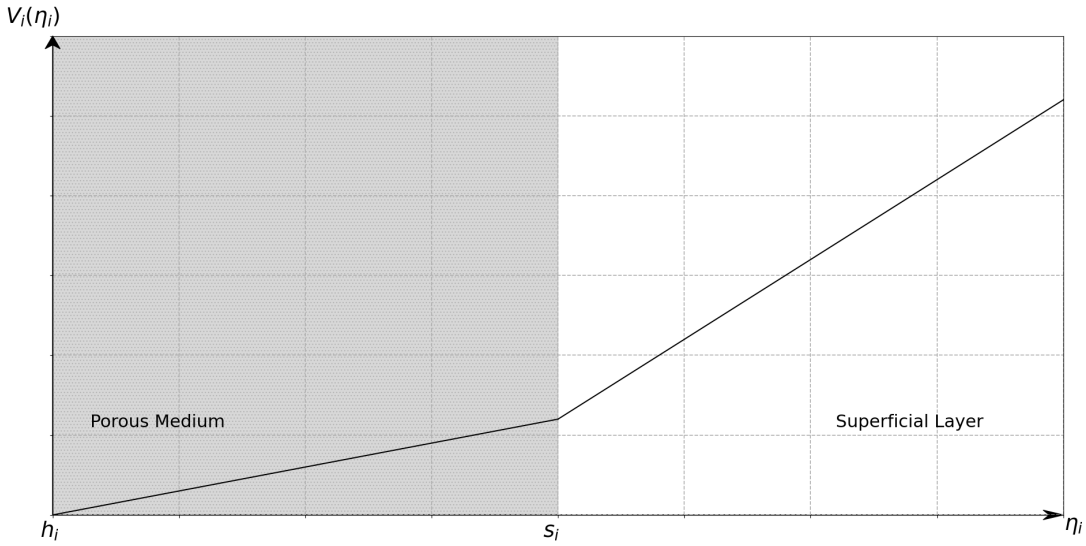

Figure 3.7 – Graphical representation of volume function.

Further investigation showed that convergence is assured for only surface or subsurface flows without additional difficulties for the algorithm. For coupled flows case, the time step reduction ensured the convergence for a longer simulation time, but not enough to complete the entire simulation period. The increase of cells in the saturation process caused the η values of these cells to oscillate between the subsurface and surface flows within the Newton algorithm iterations, resulting in the convergence problem. Weill et al. (2009) reported a similar problem. The time-step adaptative algorithm present in the Weill et al. (2009)'s model reduced the time step in this benchmark by a factor larger than ten to guarantee convergence (time step varied between 5 and 100 seconds). In the IPH-ECO hydrodynamic module developed here, there is no adaptive time-stepping algorithm implemented. So, we consider that adopting such small values of Δt becomes impractical in simulations of practical cases.

This methodology ensures strict mass conservation and avoids the negative water levels occurrence for any time step, without loss of efficiency (Volp et al., 2013; Sehili et al., 2014). This justifies the simulation conditions and results obtained by the author, despite the similarity of the algorithm of the present study.

Casulli (2015) uses a high-resolution spatial discretization using subgrids in its algorithm for the same benchmark. This approach uses two grids, a coarser grid and a high-resolution grid (sub-grid), and assumes that the cell's hydraulic parameters (e.g., roughness, wetted areas, and volume) change at the smaller scale, while the water level is uniform for the entire coarse cell (Figura 3.8) (Casulli, 2009; Cea e French, 2012; Li e Hodges, 2019). The hydraulic parameters calculated for each sub-cell will compose the parameters of the coarse cell and faces using average values (e.g., average roughness on the faces) or by integration of the wetted areas of the sub-cells (horizontal and vertical) in the coarse cell to obtain the interface areas between cells and their volumes.

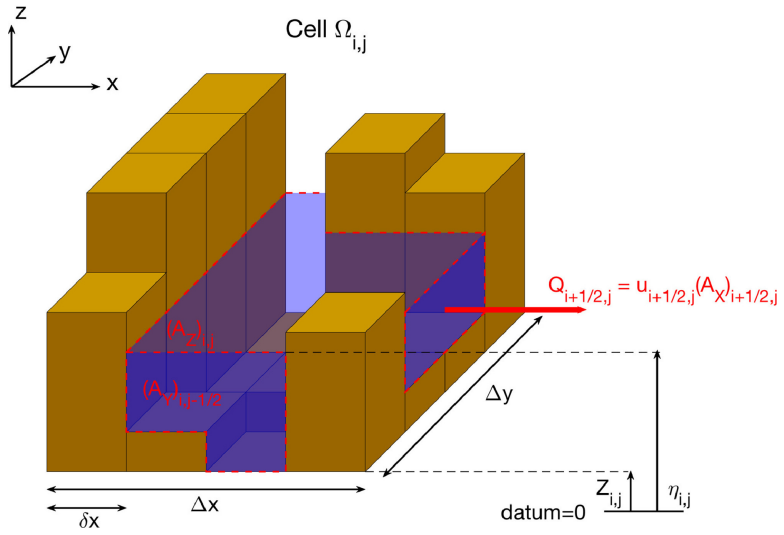

Figure 3.8 – Sub-Grid variables representation. Source: Li e Hodges (2019).

Chapter 4

Conclusion

In this study, a new approach for the hydrodynamic module of the IPH-ECO model is proposed enhancing the possibility of simulating surface flow coupled with the subsurface flow. A hybrid finite volume and finite difference approach were applied. The algorithm validation was carried out based on three benchmarks commonly applied in similar algorithms.

The results showed good agreement with available analytical and experimental results for two benchmarks tested. In the first benchmark, the flow through a porous dam under the effect of a constant hydraulic gradient and demonstrated the ability of the algorithm to simulate well-developed environmental coupled flows (steady-state). The second benchmark validated the model's capability to capture the dynamics of a coastal lagoon under tidal influence. The third benchmark simulated a tilted v-catchment with a river channel under an intense rainfall event considering two scenarios. In the first one, the surface layer was impermeable, thus allowing only surface runoff to occur. This scenario showed satisfactory results in representing runoff in the catchment and subsequent flow propagation in the river channel. A sediment layer was added below the surface level in the second scenario to assess the rainfall infiltration effect on the river channel outflow. The subsurface layer's presence caused convergence problems in Newton's algorithm when the number of cells in saturation process became larger.

The convergence problem in the third benchmark allowed the identification of limitations in the proposed algorithm. The nonlinearity arising from the cell volume equation imposes the need to adopt complementary methodologies to deal with the transition region between the flows. These methodologies ensure rigorous conservation of mass, especially for this step. Further analysis of previous studies has identified that this

process can be achieved by incorporating one of the two following methodologies:

a Adaptive Time Step in the hydrodynamic module: this methodology can optimize the entire simulation time, bringing benefits for the simulation of uncoupled surface and subsurface flows. For the simulation of coupled flows, this methodology allows the iterative time-step reduction in the transition regions, allowing more accurate estimates of the water levels in this step.

b Sub-Grid Resolution: this methodology allows estimates of roughness, wetted areas and volume with greater accuracy. These parameters are calculated at the level of the sub-cells that compose the coarse grid. The increased accuracy in estimating these parameters leads to more precise velocities, directly affecting the mass balance in the cell. The high-resolution bathymetry also enables the calculation of horizontal wetted areas and volumes with greater accuracy. This methodology smooths the transition process between flows, enabling a gradual process. This allows the algorithm to ensure a rigorous mass conservation.

The results obtained demonstrate progress towards the consolidation of the coupled hydrodynamic module between subsurface and surface flow for the IPH-ECO model. Despite the limitations identified, the results obtained allowed the definition of the subsequent steps to be taken to achieve the consolidation of the new hydrodynamic module, expanding the horizon of model applications, specifically the coupling watershed-lake modeling.

Bibliography

Ala-Aho, P., Rossi, P. M., Isokangas, E., e Kløve, B. (2015). Fully integrated surface–subsurface flow modelling of groundwater–lake interaction in an esker aquifer: Model verification with stable isotopes and airborne thermal imaging. *Journal of Hydrology*, 522:391–406.

Ala-Aho, P., Rossi, P. M., e Kløve, B. (2013). Interaction of esker groundwater with headwater lakes and streams. *Journal of hydrology*, 500:144–156.

Anderson, M. P. (2005). Heat as a ground water tracer. *Groundwater*, 43(6):951–968.

Anibas, C., Fleckenstein, J. H., Volze, N., Buis, K., Verhoeven, R., Meire, P., e Batelaan, O. (2009). Transient or steady-state? using vertical temperature profiles to quantify groundwater–surface water exchange. *Hydrological Processes: An International Journal*, 23(15):2165–2177.

Appelo, C. A. J. e Postma, D. (2004). *Geochemistry, groundwater and pollution*. CRC press.

Baskin, R. L. (1998). Locating shoreline and submarine springs in two utah lakes using thermal imagery.

Bear, J. e Verruijt, A. (2012). *Modeling groundwater flow and pollution*, volume 2. Springer Science & Business Media.

Beven, K. (2002). Towards an alternative blueprint for a physically based digitally simulated hydrologic response modelling system. *Hydrological processes*, 16(2):189–206.

Brauns, B., Bjerg, P. L., Song, X., e Jakobsen, R. (2016). Field scale interaction and nutrient exchange between surface water and shallow groundwater in the baiyang lake region, north china plain. *Journal of Environmental Sciences*, 45:60–75.

Briggs, M. A., Lautz, L. K., McKenzie, J. M., Gordon, R. P., e Hare, D. K. (2012). Using high-resolution distributed temperature sensing to quantify spatial and temporal variability in vertical hyporheic flux. *Water Resources Research*, 48(2).

Casulli, V. (1990). Semi-implicit finite difference methods for the two-dimensional shallow water equations. *Journal of Computational Physics*, 86(1):56–74.

Casulli, V. (2009). A high-resolution wetting and drying algorithm for free-surface hydrodynamics. *International Journal for Numerical Methods in Fluids*, 60(4):391–408.

Casulli, V. (2015). A conservative semi-implicit method for coupled surface–subsurface flows in regional scale. *International Journal for Numerical Methods in Fluids*, 79(4):199–214.

Casulli, V. (2017). A coupled surface-subsurface model for hydrostatic flows under saturated and variably saturated conditions. *International Journal for Numerical Methods in Fluids*, 85(8):449–464.

Casulli, V. e Cattani, E. (1994). Stability, accuracy and efficiency of a semi-implicit method for three-dimensional shallow water flow. *Computers & Mathematics with Applications*, 27(4):99–112.

Casulli, V. e Cheng, R. T. (1992). Semi-implicit finite difference methods for three-dimensional shallow water flow. *International Journal for numerical methods in fluids*, 15(6):629–648.

Casulli, V. e Walters, R. A. (2000). An unstructured grid, three-dimensional model based on the shallow water equations. *International journal for numerical methods in fluids*, 32(3):331–348.

Casulli, V. e Zanolli, P. (2010). A nested newton-type algorithm for finite volume methods solving richards' equation in mixed form. *SIAM Journal on Scientific Computing*, 32(4):2255–2273.

Casulli, V. e Zanolli, P. (2012). Iterative solutions of mildly nonlinear systems. *Journal of Computational and Applied Mathematics*, 236(16):3937–3947.

Cavalcanti, J. R., da Motta-Marques, D., e Fragoso Jr, C. R. (2016). Process-based modeling of shallow lake metabolism: Spatio-temporal variability and relative importance of individual processes. *Ecological modelling*, 323:28–40.

Cavalcanti, J. R., Dumbser, M., da Motta-Marques, D., e Junior, C. R. F. (2015). A conservative finite volume scheme with time-accurate local time stepping for scalar transport on unstructured grids. *Advances in water resources*, 86:217–230.

Cea, L. e French, J. (2012). Bathymetric error estimation for the calibration and validation of estuarine hydrodynamic models. *Estuarine, Coastal and Shelf Science*, 100:124–132.

Chen, Y., Shi, F., Kirby, J. T., Wu, G., e Liang, B. (2020). A computationally efficient subgrid model for coupled surface and groundwater flows. *Coastal Engineering*, 157:103665.

Cherkauer, D. S. e Nader, D. C. (1989). Distribution of groundwater seepage to large surface-water bodies: The effect of hydraulic heterogeneities. *Journal of Hydrology*, 109(1-2):151–165.

Choi, G.-W., Kim, G.-H., e Ahn, S.-J. (1993). On the applicable ranges of kinematic and diffusion models in open channels. Em *Hydraulic Engineering*, pgs. 803–808. ASCE.

Cunha, A. H. F., Fragoso, C. R., Chalegre, C. L. B., e Motta-Marques, D. (2020). Improvement of non-hydrostatic hydrodynamic solution using a novel free-surface boundary condition. *Water*, 12(5):1271.

Cunha, A. H. F., Fragoso, C. R., Tavares, M. H., Cavalcanti, J. R., Bonnet, M.-P., e Motta-Marques, D. (2019). Combined use of high-resolution numerical schemes to reduce numerical diffusion in coupled nonhydrostatic hydrodynamic and solute transport model. *Water*, 11(11):2288.

de Brito Jr, A. N., Fragoso Jr, C. R., e Larson, M. (2018). Tidal exchange in a choked coastal lagoon: A study of mundaú lagoon in northeastern brazil. *Regional Studies in Marine Science*, 17:133–142.

Di Giammarco, P., Todini, E., e Lamberti, P. (1996). A conservative finite elements approach to overland flow: the control volume finite element formulation. *Journal of Hydrology*, 175(1-4):267–291.

Drever, J. I. et al. (1988). *The geochemistry of natural waters*, volume 437. prentice Hall Englewood Cliffs.

Ebrahimi, K., Falconer, R. A., e Lin, B. (2007). Flow and solute fluxes in integrated wetland and coastal systems. *Environmental Modelling & Software*, 22(9):1337–1348.

Flöder, S. e Burns, C. W. (2004). Phytoplankton diversity of shallow tidal lakes: Influence of periodic salinity changes on diversity and species number of a natural assemblage 1. *Journal of Phycology*, 40(1):54–61.

Fragoso Jr, C., van Nes, E. H., Janse, J. H., e Marques, D. M. M. ("2009"). Iph-trim3d-pclake: A three-dimensional complex dynamic model for subtropical aquatic ecosystems. *Environmental Modelling & Software*, "24"("11"):"1347 – 1348".

Fragoso Jr, C. R., Marques, D. M. M., Ferreira, T. F., Janse, J. H., e van Nes, E. H. (2011). Potential effects of climate change and eutrophication on a large subtropical shallow lake. *Environmental Modelling & Software*, 26(11):1337–1348.

Genereux, D. e Bandopadhyay, I. (2001). Numerical investigation of lake bed seepage patterns: effects of porous medium and lake properties. *Journal of Hydrology*, 241(3-4):286–303.

Gunduz, O. e Aral, M. M. (2005). River networks and groundwater flow: a simultaneous solution of a coupled system. *Journal of Hydrology*, 301(1-4):216–234.

Gurrieri, J. e Furniss, G. (2004). Estimation of groundwater exchange in alpine lakes using non-steady mass-balance methods. *Journal of Hydrology*, 297(1-4):187–208.

Hagerthey, S. E. e Kerfoot, W. C. (1998). Groundwater flow influences the biomass and nutrient ratios of epibenthic algae in a north temperate seepage lake. *Limnology and Oceanography*, 43(6):1227–1242.

Hem, J. D. (1985). *Study and interpretation of the chemical characteristics of natural water*, volume 2254. Department of the Interior, US Geological Survey.

Hodges, B. R., Imberger, J., Saggio, A., e Winters, K. B. (2000). Modeling basin-scale internal waves in a stratified lake. *Limnology and oceanography*, 45(7):1603–1620.

Huang, G. e Yeh, G.-T. (2009). Comparative study of coupling approaches for surface water and subsurface interactions. *Journal of Hydrologic Engineering*, 14(5):453–462.

Janse, J. H. (2005). *Model studies on the eutrophication of shallow lakes and ditches*. Wageningen Universiteit.

Jeong, Y.-H. e Kwak, D.-H. (2020). Influence of external loading and halocline on phosphorus release from sediment in an artificial tidal lake. *International Journal of Sediment Research*, 35(2):146–156.

Jin, K.-R. e Ji, Z.-G. (2005). Application and validation of three-dimensional model in a shallow lake. *Journal of Waterway, Port, Coastal, and Ocean Engineering*, 131(5):213–225.

Kang, W.-J., Kolasa, K., e Rials, M. (2005). Groundwater inflow and associated transport of phosphorus to a hypereutrophic lake. *Environmental Geology*, 47(4):565–575.

Kenoyer, G. J. e Anderson, M. P. (1989). Groundwater's dynamic role in regulating acidity and chemistry in a precipitation-dominated lake. *Journal of Hydrology*, 109(3-4):287–306.

Kidmose, J., Engesgaard, P., Nilsson, B., Laier, T., e Looms, M. C. (2011). Spatial distribution of seepage at a flow-through lake: Lake hampen, western denmarkall rights reserved. no part of this periodical may be reproduced or transmitted in any form or by any means, electronic or mechanical, including photocopying, recording, or any information storage and retrieval system, without permission in writing from the publisher. *Vadose Zone Journal*, 10(1):110–124.

Kidmose, J., Nilsson, B., Engesgaard, P., Frandsen, M., Karan, S., Landkildehus, F., Søndergaard, M., e Jeppesen, E. (2013). Focused groundwater discharge of phosphorus to a eutrophic seepage lake (lake væng, denmark): implications for lake ecological state and restoration. *Hydrogeology Journal*, 21(8):1787–1802.

Kishel, H. F. e Gerla, P. J. (2002). Characteristics of preferential flow and groundwater discharge to shingobee lake, minnesota, usa. *Hydrological Processes*, 16(10):1921–1934.

Kollet, S. J. e Maxwell, R. M. (2006). Integrated surface–groundwater flow modeling: A free-surface overland flow boundary condition in a parallel groundwater flow model. *Advances in Water Resources*, 29(7):945–958.

Kong, J., Xin, P., Song, Z.-y., e Li, L. (2010). A new model for coupling surface and subsurface water flows: with an application to a lagoon. *Journal of Hydrology*, 390(1-2):116–120.

LaBaugh, J. W., Winter, T. C., Rosenberry, D. O., Schuster, P. F., Reddy, M. M., e Aiken, G. R. (1997). Hydrological and chemical estimates of the water balance of a closed-basin lake in north central minnesota. *Water Resources Research*, 33(12):2799–2812.

Lake, C. (2013). Simulation of climate-change effects on streamflow, lake water budgets, and stream temperature using gsflow and sntemp, trout lake watershed, wisconsin.

Lee, T. M. e Swancar, A. (1997). *Influence of evaporation, ground water, and uncertainty in the hydrologic budget of Lake Lucerne, a seepage lake in Polk County, Florida*, volume 2439. US Government Printing Office.

Lewandowski, J., Meinikmann, K., Nützmann, G., e Rosenberry, D. O. (2015). Groundwater–the disregarded component in lake water and nutrient budgets. part 2: effects of groundwater on nutrients. *Hydrological processes*, 29(13):2922–2955.

Li, Z. e Hodges, B. R. (2019). Modeling subgrid-scale topographic effects on shallow marsh hydrodynamics and salinity transport. *Advances in Water Resources*, 129:1–15.

Liang, D., Falconer, R. A., e Lin, B. (2007). Coupling surface and subsurface flows in a depth averaged flood wave model. *Journal of Hydrology*, 337(1-2):147–158.

Liang, Q., Xia, X., e Hou, J. (2016). Catchment-scale high-resolution flash flood simulation using the gpu-based technology. *Procedia Engineering*, 154:975–981.

Lou, S., Liu, S.-g., Ma, G., Zhong, G.-h., e Li, B. (2018). Fully integrated modeling of surface water and groundwater in coastal areas. *Journal of Hydrodynamics*, 30(3):441–452.

Malard, F., Plenet, S., e Gibert, J. (1996). The use of invertebrates in ground water monitoring: a rising research field. *Groundwater Monitoring & Remediation*, 16(2):103–113.

Marino, M. A. e Luthin, J. N. (1982). *Seepage and groundwater*. Elsevier.

McCarthy, M. J., Gardner, W. S., Lehmann, M. F., Guindon, A., e Bird, D. F. (2016). Benthic nitrogen regeneration, fixation, and denitrification in a temperate, eutrophic lake: Effects on the nitrogen budget and cyanobacteria blooms. *Limnology and Oceanography*, 61(4):1406–1423.

Meinikmann, K., Lewandowski, J., e Nützmann, G. (2013). Lacustrine groundwater discharge: Combined determination of volumes and spatial patterns. *Journal of Hydrology*, 502:202–211.

Munar, A. M., Cavalcanti, J. R., Bravo, J. M., da Motta-Marques, D., e Fragoso Jr, C. R. (2019). Assessing the large-scale variation of heat budget in poorly gauged watershed-shallow lake system using a novel integrated modeling approach. *Journal of Hydrology*, 575:244–256.

Munar, A. M., Cavalcanti, J. R., Bravo, J. M., Fan, F. M., da Motta-Marques, D., e Fragoso Jr, C. R. (2018). Coupling large-scale hydrological and hydrodynamic modeling: Toward a better comprehension of watershed-shallow lake processes. *Journal of hydrology*, 564:424–441.

Nakayama, T. e Watanabe, M. (2008). Missing role of groundwater in water and nutrient cycles in the shallow eutrophic lake kasumigaura, japan. *Hydrological Processes: An International Journal*, 22(8):1150–1172.

Oliveira Ommen, D. A., Kidmose, J., Karan, S., Flindt, M. R., Engesgaard, P., Nilsson, B., e Andersen, F. Ø. (2012). Importance of groundwater and macrophytes for the nutrient balance at oligotrophic lake hampen, denmark. *Ecohydrology*, 5(3):286–296.

Panday, S. e Huyakorn, P. S. (2004). A fully coupled physically-based spatially-distributed model for evaluating surface/subsurface flow. *Advances in water Resources*, 27(4):361–382.

Pereira, F., Fragoso, C., Uvo, C., e da Motta-Marques, D. (2013a). Pairing multivariate data analysis and ecological modeling in the biomanipulated lake engelsholm, denmark. *Journal of Water Management and Research*.

Pereira, F., Fragoso Jr, C., Uvo, C., Collischonn, W., e Motta Marques, D. (2013b). Assessment of numerical schemes for solving the advection–diffusion equation on unstructured grids: case study of the guaíba river, brazil. *Nonlinear Processes in Geophysics*, 20(6):1113–1125.

Pereira, F. F. (2010). Modelo hidrodinâmico e de transporte bidimensional de grade não estruturada para lagos rasos.

Pfannkuch, H. e Winter, T. (1984). Effect of anisotropy and groundwater system geometry on seepage through lakebeds: 1. analog and dimensional analysis. *Journal of Hydrology*, 75(1-4):213–237.

Ratnayake, A. S., Ratnayake, N. P., Sampei, Y., Vijitha, A., e Jayamali, S. D. (2018). Seasonal and tidal influence for water quality changes in coastal bolgoda lake system, sri lanka. *Journal of Coastal Conservation*, 22(6):1191–1199.

Rautio, A. e Korkka-Niemi, K. (2015). Chemical and isotopic tracers indicating groundwater/surface-water interaction within a boreal lake catchment in finland. *Hydrogeology Journal*, 23(4):687–705.

Rehbinder, G. e Wörman, A. (1994). Deformation of dupuit's parabola in a dam with sheet piling. *Applied scientific research*, 52(2):173–185.

Rosenberry, D. O. (2000). Unsaturated-zone wedge beneath a large, natural lake. *Water Resources Research*, 36(12):3401–3409.

Rosenberry, D. O., Lewandowski, J., Meinikmann, K., e Nützmann, G. (2015). Groundwater-the disregarded component in lake water and nutrient budgets. part 1: effects of groundwater on hydrology. *Hydrological Processes*, 29(13):2895–2921.

Santos, I. R., Niencheski, F., Burnett, W., Peterson, R., Chanton, J., Andrade, C. F., Milani, I. B., Schmidt, A., e Knoeller, K. (2008). Tracing anthropogenically driven groundwater discharge into a coastal lagoon from southern brazil. *Journal of Hydrology*, 353(3-4):275–293.

Schneider, R., Negley, T., e Wafer, C. (2005). Factors influencing groundwater seepage in a large, mesotrophic lake in new york. *Journal of Hydrology*, 310(1-4):1–16.

Sebestyen, S. D. e Schneider, R. L. (2001). Dynamic temporal patterns of nearshore seepage flux in a headwater adirondack lake. *Journal of Hydrology*, 247(3-4):137–150.

Sebok, E., Duque, C., Kazmierczak, J., Engesgaard, P., Nilsson, B., Karan, S., e Frandsen, M. (2013). High-resolution distributed temperature sensing to detect seasonal groundwater discharge into lake væng, denmark. *Water Resources Research*, 49(9):5355–5368.

Sehili, A., Lang, G., e Lippert, C. (2014). High-resolution subgrid models: background, grid generation, and implementation. *Ocean Dynamics*, 64(4):519–535.

Shaw, G. D., White, E. S., e Gammons, C. H. (2013). Characterizing groundwater–lake interactions and its impact on lake water quality. *Journal of hydrology*, 492:69–78.

Shokri, N., Montazeri Namin, M., e Farhoudi, J. (2018). An implicit 2d hydrodynamic numerical model for free surface–subsurface coupled flow problems. *International Journal for Numerical Methods in Fluids*, 87(7):343–357.

Sophocleous, M. (2002). Interactions between groundwater and surface water: the state of the science. *Hydrogeology journal*, 10(1):52–67.

Spanoudaki, K., Stamou, A. I., e Nanou-Giannarou, A. (2009). Development and verification of a 3-d integrated surface water–groundwater model. *Journal of Hydrology*, 375(3-4):410–427.

Stets, E. G., Winter, T. C., Rosenberry, D. O., e Striegl, R. G. (2010). Quantification of surface water and groundwater flows to open-and closed-basin lakes in a headwaters watershed using a descriptive oxygen stable isotope model. *Water Resources Research*, 46(3).

Sulis, M., Meyerhoff, S. B., Paniconi, C., Maxwell, R. M., Putti, M., e Kollet, S. J. (2010). A comparison of two physics-based numerical models for simulating surface water–groundwater interactions. *Advances in Water Resources*, 33(4):456–467.

Sutula, M., Day, J., Cable, J., e Rudnick, D. (2001). Hydrological and nutrient budgets of freshwater and estuarine wetlands of taylor slough in southern everglades, florida (usa). *Biogeochemistry*, 56(3):287–310.

Tang, X., Chao, J., Gong, Y., Wang, Y., Wilhelm, S. W., e Gao, G. (2017). Spatiotemporal dynamics of bacterial community composition in large shallow eutrophic lake taihu: High overlap between free-living and particle-attached assemblages. *Limnology and Oceanography*, 62(4):1366–1382.

Tian, D. e Liu, D. (2011). A new integrated surface and subsurface flows model and its verification. *Applied mathematical modelling*, 35(7):3574–3586.

Volp, N., Van Prooijen, B., e Stelling, G. (2013). A finite volume approach for shallow water flow accounting for high-resolution bathymetry and roughness data. *Water Resources Research*, 49(7):4126–4135.

Weill, S., Mouche, E., e Patin, J. (2009). A generalized richards equation for surface/subsurface flow modelling. *Journal of Hydrology*, 366(1-4):9–20.

Wetzel, R. G. (1999). Plants and water in and adjacent to lakes. *EcoHydrology: plants and water in terrestrial and aquatic environments*, pgs. 269–299.

Wilson, J. e Rocha, C. (2016). A combined remote sensing and multi-tracer approach for localising and assessing groundwater-lake interactions. *International journal of applied earth observation and geoinformation*, 44:195–204.

Winter, T. C. (1978). Numerical simulation of steady state three-dimensional groundwater flow near lakes. *Water Resources Research*, 14(2):245–254.

Winter, T. C. e Likens, G. E. (2009). *Mirror lake: Interactions among air, land, and water*, volume 2. Univ of California Press.

Winter, T. C., Rosenberry, D. O., e LaBaugh, J. W. (2003). Where does the ground water in small watersheds come from? *Groundwater*, 41(7):989–1000.

Wu, R., Chen, X., Hammond, G., Bisht, G., Song, X., Huang, M., Niu, G.-Y., e Ferre, T. (2021). Coupling surface flow with high-performance subsurface reactive flow and transport code pflotran. *Environmental Modelling & Software*, 137:104959.

Xin, P., Yuan, L.-R., Li, L., e Barry, D. A. (2011). Tidally driven multiscale pore water flow in a creek-marsh system. *Water Resources Research*, 47(7).

Xu, H., Zhang, L., Shang, J., DAI, J., e FAN, C. (2009). Denitrification and anammox on the sediment-water interface in the meiliang bay of lake taihu. *J Lake Sci*, 21(6):775L781.

Yihdego, Y. e Becht, R. (2013). Simulation of lake–aquifer interaction at lake naivasha, kenya using a three-dimensional flow model with the high conductivity technique and a dem with bathymetry. *Journal of Hydrology*, 503:111–122.

Yuan, B., Yuan, D., Sun, J., e Tao, J. (2012). A finite volume model for coupling surface and subsurface flows. *Procedia Engineering*, 31:62–67.

Yuan, D., Lin, B., e Falconer, R. (2008). Simulating moving boundary using a linked groundwater and surface water flow model. *Journal of hydrology*, 349(3-4):524–535.

Yuan, L.-R., Xin, P., Kong, J., Li, L., e Lockington, D. (2011). A coupled model for simulating surface water and groundwater interactions in coastal wetlands. *Hydrological Processes*, 25(23):3533–3546.

Zhou, S., Kang, S., Chen, F., e Joswiak, D. R. (2013). Water balance observations reveal significant subsurface water seepage from lake nam co, south-central tibetan plateau. *Journal of Hydrology*, 491:89–99.

Zhu, C. e Schwartz, F. W. (2011). Hydrogeochemical processes and controls on water quality and water management. *Elements*, 7(3):169–174.

Zhu, G., Wang, S., Wang, W., Wang, Y., Zhou, L., Jiang, B., Den Camp, H. J. O., Risgaard-Petersen, N., Schwark, L., Peng, Y., et al. (2013). Hotspots of anaerobic ammonium oxidation at land–freshwater interfaces. *Nature Geoscience*, 6(2):103–107.